Barremian–early Aptian charophyte biostratigraphy revisited

Jordi Pérez-Cano[1*], Telm Bover-Arnal[2,3], and Carles Martín Closas[1]

[1] Departament de Dinàmica de la Terra i de l'Oceà, Facultat de Ciències de la Terra, Institut de Recerca de la Biodiversitat (IRBio), Universitat de Barcelona-UB, 08028 Barcelona, Catalonia, Spain

[2] Departament de Mineralogia, Petrologia i Geologia Aplicada, Facultat de Ciències de la Terra, Universitat de Barcelona-UB, 08028 Barcelona, Catalonia, Spain

[3] Institut de Recerca GEOMODELS, c/ Martí Franquès s/n, 08028 Barcelona, Catalonia, Spain

*Corresponding author: jordi_perez-cano@ub.edu

Abstract

New Barremian–early Aptian charophyte biozonations are proposed here based on the charophyte succession in the Maestrat Basin (Iberian Chain, Spain). Biostratigraphic analysis distinguished two biozonations, European and Eurasian, which were compared to establish correlations. This is the first time that Early Cretaceous charophyte biozones are calibrated by means of strontium-isotope stratigraphy, enabling their correlation with the coeval marine realm (ammonite biostratigraphy). The European charophyte biozonation is formed of two partial range biozones, whose index species were endemic from the Cretaceous Tethyan Archipelago (present-day Europe and Northern Africa): (1) Globator maillardii var. trochiliscoides (early Barremian) and (2) Ascidiella cruciata-Pseudoglobator paucibracteatus. The base of the A. cruciata-P. paucibracteatus biozone was calibrated with an oyster shell sample whose $^{87}Sr/^{86}Sr$ is 0.707482, translating to a late early Barremian age. The total time span of this latter biozone is late early Barremian–early Aptian. The Eurasian biozonation involves a novel Lower

Cretaceous charophyte biostratigraphy. It has more resolution than the European biozonation, as it is composed of three partial range biozones whose index species were well-distributed in Eurasia. From oldest to youngest these are: (1) Atopochara trivolvis var. triquetra, (2) Hemiclavator neimongolensis var. neimongolensis, and (3) Clavator grovesii var. jiuquanensis. The A. trivolvis var. triquetra biozone characterises the early Barremian, being almost equivalent to the European G. maillardii var. trochiliscoides biozone. The base of the H. neimongolensis var. neimongolensis biozone is marked by the first appearance datum (FAD) of *Hemiclavator neimongolensis* var. *neimongolensis* and was calibrated with an oyster shell whose $^{87}Sr/^{86}Sr$ is 0.707481 corresponding to a late early Barremian age. The top of the H. neimongolensis var. neimongolensis biozone coincides with the FAD of *Clavator grovesii* var. *jiuquanensis*. The base of the C. grovesii var. jiuquanensis biozone was dated with an oyster sample sample collected 25 m below the FAD of *C. grovesii* var. *jiuquanensis*. The $^{87}Sr/^{86}Sr$ value of this sample is 0.707489, which translates into an early late Barremian age. Thus, the H. neimongolensis var. neimongolensis biozone spans the late early Barremian-early late Barremian interval. The top of the Clavator grovesii var. jiuquanensis biozone (late Barremian–early Aptian) is marked by the FAD of *Clavator grovesii* var. *lusitanicus*. The newly proposed Eurasian charophyte biozonation will facilitate the correlation between non-marine basins in one of the largest continental areas on Earth.

Keywords: Charophyta, Clavatoraceae, Lower Cretaceous, Iberia, China, Intercontinental correlation, Biochronology

1. Introduction

The fructifications (utricles) of the fossil charophyte family Clavatoraceae are widely used for the biostratigraphic characterisation of continental Late Jurassic-Early

Cretaceous successions (e.g., Grambast 1974, Wang and Lu 1982, Mussacchio 1989, 2000, Schudack 1987, 1993, Martín-Closas 1989, Martín-Closas and Alonso-Millán 1998, Feist et al. 1995, Trabelsi et al. 2016). A number of Baremian-lower Aptian charophyte biozonations have been proposed in Europe (e.g., Grambast 1974; Feist et al. 1995, Riveline et al. 1996, Mojon 1996, 2002) and China (e.g., Wang and Lu 1982, Peng et al. 2003, Yang et al. 2008). Despite the extensive work carried out on clavatoracean biostratigraphy in Europe and Asia, the different biozones proposed have not been numerically dated or correlated between continents. The relative ages of previous proposals were determined from the correlation with foraminifera found in marine deposits, which occur interbedded within continental successions (e.g., Combes et al. 1966, Martín-Closas and Salas, 1988, 1994,, Mojon 2002, Martín-Closas et al. 2009). Li et al. (2020) dated charophyte assemblages from Chinese basins to the late Barremian-early Aptian time by using previously published chemostratigraphic data and by considering the age assigned to similar charophyte assemblages in European basins.

In Europe, two Barremian biozones were first proposed by Grambast (1974) spanning the early Barremian and the late Barremian, respectively. These biozones were the bases for the later proposals (e.g., Feist et al. 1995, Mojon 1996). The most used present-day European Barremian biozonation was proposed by Riveline et al. (1996) and later modified by Martín-Closas et al. (2009). These authors used assemblages and ages similar to those reported by Grambast (1974).

In Asia, different charophyte biostratigraphic charts have been proposed for the Chinese basins. Wang and Lu (1982) defined two biozones that have Hauterivian-early Barremian and late Barremian age ranges, respectively. Later on, Peng et al. (2003) combined these two biozones into a single biozone spanning the whole Barremian, and Yang et al. (2008) considered this latter biozone to also span the Hauterivian Stage. This relatively low-resolution charophyte biostratigraphy contrasts with the proposals

for other Cretaceous stages whose time span is similar to that of the Barremian. This is the case, for example, with the late Campanian-late Maastrichtian European and Asian charophyte biostratigraphy that involve three biozones (e.g., Vicente et al. 2015, Li et al. 2019).

This paper presents new European and Eurasian charophyte biostratigraphic frameworks for the Barremian-early Aptian, based on the clavatoracean succession identified in the Maestrat Basin (Iberian Chain, Spain) and the extensive data on clavatoracean biogeography available for this time span elsewhere (e.g., Martín-Closas and Wang 2008, Martín-Closas 2015, Pérez-Cano et al. 2020). The analysis of this charophyte record along with a continuous Barremian succession enabled us to determine the first appearance datum (FAD) of several species from the Barremian, improving the resolution of the Barremian biostratigraphy. Moreover, the identification of the FAD of Eurasian-distributed taxa (i.e., *Atopochara trivolvis* var. *triquetra*, *Clavator grovesii* var. *jiuquanensis*, *C. harrisii*, *C. calcitrapus*, and *Hemiclavator neimongolensis* var. *neimongolensis*; Martín-Closas and Wang 2008, Martín-Closas 2015) enabled their use as index species, improving the correlation between Europe and Asia.

The utility of a biostratigraphic framework increases when it is faithfully calibrated to a time scale. Charophyte biozonations from other ages have been calibrated against the Geomagnetic Polarity Time Scale (GPTS), which translates into numerical ages. This has been performed for the Campanian–Danian charophyte biozonations of the Pyrenees (Galbrun et al. 1993, Vicente et al. 2015) and the Chinese basins (Li et al. 2016, 2019), as well as for the Eocene biozonation of the Ebro Basin (Sanjuan et al. 2014). However, the calibration of Late Jurassic-Early Cretaceous charophyte biozones in southern European basins with the GPTS is not straightforward due to the Alpine Orogeny-related remagnetisation of the Mesozoic record (e.g.,

106 Moreau et al. 1992, Gong et al. 2009). Consequently, the calibration of the Barremian-
107 early Aptian biostratigraphy presented here was performed by numerically dating
108 marine intercalations using strontium isotope stratigraphy (SIS), a methodology
109 extensively used for the calibration of marine records (e.g., Steuber 1999, Williamson et
110 al. 2012, Frijia et al. 2015, Bover-Arnal et al. 2016, Caus et al., 2016).
111
112 **2. Geological setting**
113 The Maestrat Basin was part of an intracratonic rift system that developed in the
114 NE part of the Iberian plate (Fig. 1A–B) during the Mesozoic as a consequence of the
115 breakup of Pangaea and the opening of the Central Atlantic Ocean (Salas and Casas
116 1993, Salas et al. 2001). According to Salas et al. in Martín-Chivelet et al. (2019), there
117 were three different stages of rifting followed by three post-rift phases in the Iberian rift
118 system: (1) Late Permian–Triassic rifting, (2) Early–Middle Jurassic post-rift, (3) Late
119 Jurassic–middle Berriasian rifting, (4) late Berriasian–Hauterivian post-rift, (5)
120 Barremian–early Albian rifting and (6) Late Cretaceous post-rift. The Maestrat Basin is
121 associated with the Late Jurassic–middle Berriasian and the Barremian–early Albian
122 rifting stages. Listric extensional faults and palaeotopographic highs subdivided the
123 basin into several sub-basins, from north to south, namely El Perelló, Morella, Oliete,
124 Las Parras, Galve, Salzedella, Orpesa, Penyagolosa and Cedramán, with different
125 subsidence rates and sedimentary features (Fig. 1B; Salas and Guimerà 1996, Salas et
126 al. in Martín-Chivelet et al. 2019). The study areas are located within the Morella Sub-
127 basin (Fig. 1B–D). The sedimentary deposition in this sub-basin ranged from non-
128 marine carbonate successions, mainly found along the northern margin of the half-
129 graben, to hemipelagic successions occurring in the central zone of the sub-basin
130 (Canérot et al. 1982, Salas 1987). Later, during the Alpine orogeny (Late Cretaceous–

131 early Miocene), the Iberian rift system was inverted to form the Iberian Chain (Nebot
132 and Guimerà 2016, Guimerà 2018).
133
134 ----------Please insert Fig. 1 near here----------
135
136 The Barremian sedimentary record of the Morella Sub-basin is subdivided into
137 five formations: Cantaperdius, Artoles, Morella, Cervera del Maestrat and Xert (Fig. 2;
138 Canérot et al. 1982, Salas 1987, Salas et al. 2001, Bover-Arnal et al. 2016). The present
139 study was carried out along the Cantaperdius, Artoles and Morella formations (Fig. 2).
140 The non-marine lacustrine Cantaperdius Formation is mainly composed of alternating
141 charophyte-rich marls and limestones. It is up to 400 m-thick in the northern area of the
142 Morella Sub-basin and becomes thinner towards the central part of the basin, where it
143 laterally changes into the Artoles Formation. The Artoles Formation, which also
144 overlies the Cantaperdius Formation throughout the sub-basin, is characterized by
145 coastal to shallow open marine marls and limestones rich in oysters (Salas 1987, Salas
146 et al. 2001, Bover-Arnal et al. 2016). This unit is up to 700 m thick in the central parts
147 of the sub-basin, with its thickness decreasing to less than 200 m in the marginal areas.
148 Laterally and above the Artoles Formation, there is the Morella Formation, a non-
149 marine unit composed of grey to red and purple clays and sandstones (Canérot et al.
150 1982, Salas, 1987, Gàmez et al., 2003). Towards the depocentre of the sub-basin, the
151 Morella Formation becomes progressively more brackish-influenced, laterally passing
152 to the Cervera del Maestrat Formation that contains mixed carbonate-siliciclastic coastal
153 and shallow marine deposits (Canérot et al. 1982, Salas, 1987, Salas et al. 2001). The
154 Xert Formation corresponds to a fully marine succession composed of marls and
155 limestones rich in orbitolinids. The Morella, Cervera del Maestrat and Xert formations

156 have been dated to the late Barremian using ammonites and SIS (García et al. 2014,
157 Bover-Arnal et al. 2016).
158
159 ----------Please insert Fig. 2 near here----------
160
161 **3. Palaeobotanical setting**
162 Since the middle of the 20th century, the taxonomic studies carried out by Louis
163 Grambast (Grambast 1966a, b, 1967, 1968, 1969, 1970, 1974) and later continued by
164 Martín-Closas and Grambast-Fessard (1986), Martín-Closas (1989, 2000), Schudack
165 (1993), Climent-Domènech et al. (2009) and Pérez-Cano et al. (2020) have illustrated
166 the high biodiversity of the charophytes occurring in the Lower Cretaceous non-marine
167 record of the Maestrat Basin. These studies showed that the extinct Clavatoraceae
168 family dominated the non-marine settings of the basin during that period. The
169 stratigraphic continuity of the non-marine record of the Maestrat Basin provides an
170 excellent context to understand the evolution and phylogeny of the clavatoracean
171 species, enabling the identification of evolutionary lineages with biostratigraphic
172 significance (Grambast, 1966a, 1968, 1974; Martín-Closas, 1989, 1996, 2000). The
173 species identified in the studied sections are summarised in Table 1 and shown in Plates
174 1 and 2.
175 ----------Please insert Table 1 near here----------
176
177 **4. Materials and methods**
178 **4.1. Lithostratigraphy and charophyte sampling**
179 Two Barremian sections from the Morella Sub-basin were logged and
180 systematically sampled for the identification of charophyte assemblages: Herbers-Mas
181 de Petxí (base: 40º42’39”N, 0º0’36”W; top: 40º42’34”N, 0º0’30”E) (Figs. 1C and 3A–

B) and Fredes (base: 40°41'20.71"N, 0°10'1.25"E; top: 40°41'27.09"N, 0°9'54.44"E) (Figs. 1D and 4). Samples of approximately 3 kg were taken from each marl or clay bed. In the laboratory, the samples were disaggregated using a solution of water, sodium carbonate (Na_2CO_3; useful for deflocculating the clay), and hydrogen peroxide (H_2O_2; eliminates the organic matter and helps with the disaggregation). These samples were left for a few days and then sieved through meshes with apertures of 1, 0.5, and 0.2 mm. When the samples were dried, charophyte fructifications were handpicked using a Wild M5A binocular microscope. The fructifications were measured using a Motic BA310 microscope and the Motic Images Plus 2.0 software. Selected specimens were studied and photographed with a Quanta 200 Scanning Electronic Microscope (SEM) at the Centres Científics i Tecnològics de la Universitat de Barcelona (CCiTUB). The figured specimens were deposited at the Museu de Geologia del Seminari Conciliar de Barcelona (MGSCB). The handpicked material has been kept at the Departament de Dinàmica de la Terra i de l'Oceà of the Universitat de Barcelona.

Limestone beds were also sampled and studied as *c*. 30 µm-thick sections cut parallel and perpendicular to the bedding surface of the sample. These sections were studied and photographed with a Motic BA 310 petrographic microscope.

----------Please insert Plate 1 near here----------

----------Please insert Plate 2 near here----------

4.2. Trace element concentration and strontium-isotope analysis

Eleven oyster shells were sampled for SIS. Four oysters were obtained from the Fredes section, all of them belonging to the Cantaperdius Formation (Fig. 4). In the Herbers-Mas de Petxí section, six oyster samples were collected from the Artoles

Formation and one sample was gathered from the upper part of the Morella Formation close to the top of the non-marine record (Fig. 3A–B).

Oyster shells were cleaned to remove superficial contamination and later polished and screened for diagenetic changes. Visual inspection of the shells helped to prevent the sampling of bioperforated parts, cements, and other alterations within the shell structure. The externally non-altered parts of the shells were sampled with a hand-operated microdrill equipped with a tungsten drill bit (0.3 to 0.5 mm in diameter) and homogenised in an agate mortar mill. The resulting carbonate powder from each shell was divided into two samples of ~100 mg. The first sample was employed for the Inductively Coupled Plasma-Optical Emission Spectroscopy (ICP-OES) analysis of Ca, Sr, Mg, Fe and Mn concentrations in order to perform diagenetic screening. This was carried out at the Centres Científics i Tecnològics de la Universitat de Barcelona (CCiTUB). The second sample was used for SIS, which was performed at the Unidad de Geocronología, CAI de Ciencias de la Tierra y Arqueometría at the Universidad Complutense de Madrid (Spain). Strontium (Sr) was separated from the sample by standard ion-exchange resin methods. The Sr isotope ratios ($^{87}Sr/^{86}Sr$) were measured on a TIMS-Phoenix® mass spectrometer. The analysis was corrected to avoid interferences from ^{87}Rb, and the $^{87}Sr/^{86}Sr$ ratio was normalised to the mean value of 0.1194. The analysed raw results were corrected using the standard NBS 987, which has a value of 0.710249 ± 0.000012 (2 statistical uncertainty, $n = 7$).

5. Stratigraphy and sedimentology

A sedimentological analysis was performed in the Herbers-Mas de Petxí and Fredes sections to determine the relationship between the presence or absence of charophyte species and the depositional facies. Taphonomical features such as fragmentation and abrasion, as well as the occurrence of different charophyte organs

233 together or even connected anatomically (i.e., fructifications and thalli), were
234 investigated to elucidate the degree of autochthony or allochthony of the charophyte
235 remains in the sedimentary record.
236
237 **5.1. The Herbers-Mas de Petxí section**
238 This section crops out to the south and south-east of the village of Herbers
239 (Castelló, Spain; Fig. 1C) and contains an 800 m-thick continuous Barremian
240 succession. The present study focuses on the lower 690 m, corresponding to the
241 Cantaperdius, Artoles, and Morella formations (Figs. 2 and 3A–B).
242 The Barremian succession is deposited above an irregular karstified surface
243 exhibiting vertical tubular structures that are interpreted as root marks marking the top
244 of the Hauterivian Herbers Formation (Fig. 2). The lowermost part of the Barremian
245 record (0–11 m), which corresponds to the base of the Cantaperdius Formation, consists
246 of variegated clays that change from a greyish colour at the base to a yellowish colour in
247 the middle and a reddish colour at the top. Similar deposits at the base of the Barremian
248 record in the Iberian Chain have been interpreted as laterite deposits (Combes 1969).
249 These clays contain charophyte remains (thalli and fructifications), ostracods and
250 molluscan fragments. Up to 0.5 m-thick packstones occur, interbedded with the clays.
251 The charophyte assemblage in the clays is mainly composed of utricles of well-
252 preserved *Atopochara trivolvis* var. *triquetra*, *Clavator harrisii* var. *harrisii*, *Ascidiella*
253 *stellata* var. *stellata* and *A. triquetra*, as well as gyrogonites of aff. *Mesochara harrisii*.
254 Charophyte thalli portions, *Munieria grambastii* Bystrický and *Favargerella aquavivae*
255 Martín-Closas et Salas, have been also observed, suggesting that the charophyte
256 assemblage is autochthonous. Utricles of *Hemiclavator adnatus* and *H. neimongolensis*
257 var. *posticecaptus* are rare and occur abraded. They are therefore interpreted as

allochthonous components. Above these clays, the section has been divided into eight descriptive intervals, from A to H (see Fig. 3A-B).

Interval A (11–161.5 m) mainly consists of charophyte-rich massive dark-grey limestones and marls that are stacked in parasequences. The marls are frequently absent from the parasequences, but when they do occur, they consist of thin (<20 cm) layers that contain abundant clavatoracean utricles associated with thalli and ostracods. The marls are interbedded with limestones whose texture varies among mudstone, wackestone and packstone and contain abundant clavatoracean utricles and thalli, ostracods, and black pebbles (<1 mm across). These limestones often show colour mottling. The top of the packstones is characterised by the presence of root marks. Successions with these sedimentary features have been attributed to shallow carbonate lakes laterally associated with palustrine environments (see, e.g., Gierlowski-Kordesch 2010, Alonso-Zarza and Wright 2010). Similar sedimentary settings have been described by Platt (1989) and Meléndez et al. (2009) in other parts of the Lower Cretaceous Iberian Chain.

The charophyte assemblages in this interval are mainly of *A. trivolvis* var. *triquetra*, *Clavator harrisii* var. *dongjingensis*, var. *harrisii*, and var. *reyi*, *Ascidiella stellata* var. *stellata*, and var. *lata*, *A. triquetra* and, rarely, *Globator maillardii* var. *trochiliscoides*, *Hemiclavator adnatus*, *H. neimongolensis* var. *posticecaptus*, aff. *Mesochara harrisii* and *Porochara maestratica*. Most samples contain well-preserved fructifications that are associated with the charophyte thalli of *F. aquavivae*, *Clavatoraxis* sp., *Charaxis* sp., and *M. grambastii*. Utricles of the genus *Ascidiella* are locally found attached to *F. aquavivae* thalli portions while *C. harrisii* var. *harrisii*, *H. adnatus* and *H. neimongolensis* var. *posticecaptus* are attached to *Clavatoraxis* sp. phylloids. Taphonomic data show that these assemblages can be regarded as autochthonous. Populations of *P. maestratica* are frequently small, but, locally, this

284 species can dominate charophyte assemblages. Porocharacean-rich autochthonous
285 assemblages from the Lower Cretaceous are interpreted as evidence of brackish water
286 conditions (e.g., Martín-Closas and Grambast-Fessard 1986, Schudack 1993, Climent-
287 Domènech et al. 2009).

288 **Interval B** (161.5–187 m) is formed of interbedded marls and limestones, with
289 the marl beds being more abundant and thicker than those in Interval A. The marl layers
290 are <50 cm thick and contain abundant charophyte thalli and fructifications (utricles and
291 gyrogonites), ostracods, gastropods and, rarely, small agglutinated benthic foraminifera.
292 Limestones are up to 1 m-thick and exhibit wackestone and packstone textures with a
293 palaeontological content similar to that observed in the limestones of Interval A. Root
294 marks at the top of the limestone beds also occur, suggesting deposition in very shallow
295 lake and palustrine environments (cf. Alonso-Zarza and Wright 2010). As in Interval A,
296 Interval B presents indications of lacustrine deposition with scarce palustrine
297 intercalations and a low exposition rate. However, the thicker marl layers in Interval B
298 compared to Interval A suggests that the freshwater alkaline lakes received higher
299 clastic input than those described for Interval A (e.g., Meléndez et al. 2009).

300 The charophyte assemblage in this interval is similar to that observed in the
301 interval A (Fig. 3A). The only differences are the first occurrences of *Echinochara*
302 *lazarii* and, locally, *Globator maillardii* var. *biutricularis*. Moreover, *G. maillardii* var.
303 *trochiliscoides* is more frequent and abundant here than in the underlying interval. The
304 last occurrences of *A. stellata* var. *stellata* and *Hemiclavator adnatus* are also recorded
305 in this interval. Most samples contain well-preserved fructifications that are associated
306 with thalli, suggesting autochthony. However, the gyrogonites of *P. maestratica* and the
307 benthic foraminifera are frequently broken and/or abraded, which indicates lateral
308 transport.

309

----------Please insert Fig. 3A near here----------

Interval C (187−276 m) is mainly composed of a succession of clavatoracean-rich mudstone to packstones, resulting in a crest landscape. Occasionally, the limestones are interbedded with <20 cm-thick marl beds. The palaeontological content of the limestones and marls is similar to that of Interval A. They also show intraclasts and root marks at the top, sedimentary features that indicate lakeshore environments (e.g., Gierlowski-Kordesch 2010; Alonso-Zarza and Wright 2010).

The charophyte assemblages in this interval are composed of *E. lazarii*, *A. trivolvis* var. *triquetra*, *C. harrisii* var. *harrisii*, and var. *reyi*, *Ascidiella stellata* var. *lata*, *A. triquetra*, *H. neimongolensis* var. *posticecaptus* and *H. neimongolensis* var. *neimongolensis* and gyrogonites of *P. maestratica* and aff. *M. harrisii*. They are mostly formed of well-preserved fructifications associated with thalli, indicating that the observed charophyte remains are autochthonous. The occurrence of porocharacean-dominated limestones interbedded with clavatoracean-rich limestones is interpreted as evidence of brackish water environments laterally associated with freshwater lakes, similar to Interval A.

Interval D (276–366 m) is another interval with abundant marl and comprises the uppermost part of the Cantaperdius Formation and the lowermost part of the Artoles Formation. The lower part of the interval (276–348 m) is composed of a monotonous succession of interbedded marls and packstones. While marls contain abundant charophyte fructifications and thalli, ostracods, and gastropods, limestones contain abundant charophyte thalli (mainly *M. grambastii*), few charophyte fructifications, and large intraclasts (>1 cm in diameter). Root marks and ferruginous surfaces are common at the top of the limestones. The facies slightly change in the upper part of the interval (348–366 m). The marls of this upper part contain abundant, but poorly diverse

clavatoracean utricles, together with small agglutinated benthic foraminifera, and few ostracods. These marls are interbedded with mudstone-wackestone limestones containing a few charophyte utricles and thalli as well as ostracods. They are also occasionally interbedded with oyster-bearing packstones. The lower part of the interval is interpreted as deposited in a lacustrine setting. The root-marked limestones correspond to lakeshore areas surrounded by a palustrine zone, similar to those described by Meléndez et al. (2009) and Alonso-Zarza and Wright (2010) in other Lower Cretaceous Iberian basins. Upwards, the succession shows a progressive substitution of the freshwater lake facies by the brackish and oyster-bearing coastal marine deposits of the Artoles Formation (Fig. 2), which mark the onset of the early Barremian transgression in the basin (Bover-Arnal et al. 2016).

The charophyte assemblages of Interval D are mainly composed of *E lazarii*, *G. maillardii* var. *trochiliscoides*, and var. *biutricularis*, *A. trivolvis* var. *triquetra* , *C. harrisii* var. *dongjingensis* (last occurrence), var *harrisii*, and var. *reyi*, *Clavator calcitrapus* var. *jiangluoensis*, and var. *calcitrapus* (first occurrence), *Hemiclavator neimongolensis* var. *neimongolensis*, and aff. *M. harrisii.* Occasionally, they also include *Ascidiella stellata* var. *lata*, *A. triquetra*, *H. neimongolensis* var. *posticecaptus* (last occurrence) and *P. maestratica*. Most samples show well-preserved utricles and gyrogonites, occasionally attached to thalli. They are thus considered to be autochthonous. The gyrogonites of *P. maestratica* show abrasion, indicating reworking or lateral transport.

Interval E (366–450 m) represents the lower part of the Artoles Formation (Fig. 3B). It begins with 30 m of interbedded marls and wackestone limestones rich in well-preserved gyrogonites of *P. maestratica*, small agglutinated benthic foraminifera, and ostracods, indicating brackish water settings, as interpreted for Intervals A and C. The marl layers can also contain scarce utricles of *E. lazarii*. These porocharacean-rich beds

362 are overlaid by 54 m of mudstone to packstones that contain agglutinated benthic
363 foraminifera, miliolids, oyster shells, gastropods, and rare porocharacean gyrogonites.
364 In these facies, porocharacean gyrogonites are slightly abraded, suggesting lateral
365 transport. These marine limestones are interpreted as shallow water facies that were
366 deposited in marginal coastal areas of a carbonate shelf (e.g., Tucker 1985).
367 Accordingly, Interval E shows an evolution of depositional environments from brackish
368 water settings dominated by porocharaceans at the base to shallow marine settings at the
369 top.

370 **Interval F** (450–490 m) belongs to the Artoles Formation at the base and to the
371 Morella Formation at the top (Fig. 3B). The lower 28 m (450–478 m) are composed of
372 >2 m-thick marls interbedded with 0.5–1 m-thick limestones. The palaeontological
373 assemblage found in the marls includes abundant charophyte thalli and clavatoracean
374 fructifications, ostracods, and molluscs. The limestones contain ostracods, gastropods,
375 bivalves, dasycladaleans, benthic foraminifera, and rare clavatoracean fructifications
376 and thalli. The top of the limestones is characterised by a ferruginous hardground
377 surface, locally encrusted by oysters. The upper 12 m (478–490 m) of the interval
378 shows a very distinct facies succession, characterised by repetitive interbedded grey and
379 red clays. These clays contain abundant and diverse charophytes associated with
380 ostracods, gastropods, and lituolid foraminifera. The lithofacies have strong similarities
381 with those described by Gàmez et al. (2003) for the Morella Formation in the
382 depocentre of the Maestrat Basin (Salzedella Sub-basin; Fig. 1B). Consequently, these
383 clays are ascribed to the Morella Formation. The depositional setting of Interval F is
384 interpreted to have evolved from marginal coastal marine settings in the lower 28 m and
385 from brackish non-marine environments in the upper 12 m.

386 The charophyte assemblages are rich in *E. lazarii*. Less abundant charophytes
387 include *G. maillardii* var. *trochiliscoides*, and var. *biutricularis*, *A. trivolvis* var.

388 *triquetra*, *C. harrisii* var. *reyi*, *Ascidiella cruciata* (first occurrence), *H. neimongolensis*
389 var. *neimongonlensis*, *Pseudoglobator paucibracteatus* (first occurrence), aff. *M.*
390 *harrisii*, and *P. maestratica*. Fertile whorls of *E. lazarii* are frequently preserved, and
391 two utricles were found anatomically attached the corrresponding thalli, i.e., *Charaxis*
392 *spicatus* Martín Closas et Diéguez, suggesting autochthony. The other fructifications of
393 the assemblage (*G. maillardii* var. *trochiliscoides* and var. *biutricularis*, *A. trivolvis* var.
394 *triquetra*, *C. harrisii* var. *harrisii* and var. *reyi*, *A. cruciata*, *H. neimongolensis* var.
395 *neimongolensis*, *P. paucibracteatus,* aff. *M. harrisii* and *P. maestratica*) are well-
396 preserved or slightly eroded, which suggests parautochthony.
397
398 ----------Please insert Fig. 3B near here----------
399
400 **Interval G** (490–611 m) corresponds to the upper part of the Artoles Formation in
401 the Herbers-Mas de Petxí section (Fig. 3B). It mainly consists of marls alternating with
402 cross-bedded packstone-grainstone limestones. The marls frequently contain bivalve
403 moulds. The limestones are lenticular and show a lateral thinning from 2 m in the
404 central parts to 0.3 m at the edges of the bed. The bioclastic components of the
405 limestones mainly correspond to oysters, gastropods, echinoids, dasycladales, and
406 benthic foraminifera. At the base, the limestone beds contain abundant mud pebbles.
407 The occurrence of cross-bedding, lateral thinning of the beds, and the presence of
408 intraclasts at the base, indicates that these limestones correspond to channel-fill deposits
409 formed in shallow marine settings (e.g., Tucker 1985, Bover-Arnal and Strasser 2013).
410 Above the channelised beds, a 7 m-thick laminated mudstone limestone with thin
411 calcified filaments occurs. The laminas of this mudstone are a millimetre-thick and
412 contain benthic foraminifera and very small mollusc bioclasts. This deposit represents a
413 microbial algal mat formed in intertidal to shallow subtidal areas, resembling the one

reported by Tucker (1985) and Bover-Arnal and Strasser (2013). Thus, the interval is attributed to a deposition in a tidal flat.

The charophyte assemblages of this interval are mainly composed of well-preserved utricles of *Echinochara lazarii*, which are considered autochthonous. Small populations of *G. maillardii* var. *biutricularis* and *A. cruciata* are well-preserved to slightly eroded, suggesting parautochthony.

Interval H (611–680 m) is ascribed to the Morella Formation, being the second interval attributed to this formation in Herbers-Mas de Petxí (Fig. 3B). It starts with a 1 m-thick red clay interval followed by a 1.5 m-thick charophyte-rich limestone. The following 37 m are characterised by up to 5 m-thick layers of variegated clays (grey, red, ochre, and purple) that contain abundant charophyte remains (thalli and fructifications), ostracods, and agglutinated benthic foraminifera. Red and purple clays show mottled areas and contain abundant root marks. Thin (3–20 cm-thick) wackestone-packstones occur, interbedded with the clays. These limestones are rich in charophyte utricles and thalli, found sometimes anatomically connected, as well as ostracods and molluscs. The uppermost 30.5 m of the interval (649.5–680 m) are composed of a succession of grey and red clays interbedded with packstones that are rich in oysters and ostracods and frequently exhibit bioturbated tops. The microfossil content of the clays resembles that of the basal part of the interval, mainly containing charophyte fructifications and thalli, ostracods, and agglutinated benthic foraminifera. The top of this stratigraphic interval is marked by a 2 m-thick, cross-bedded and bioturbated packstone limestone rich in bivalve fragments and ostracods, similar to the channel-fill deposits observed in the underlying interval.

Similar clay-dominated deposits occur in the type locality of the Morella Formation, where they are associated with conglomerates and sands, thus being interpreted as deposited in a mudflat environment (Gàmez et al. 2003). In the studied

section, lacustrine limestones occur interbedded with clays and sandstone, unlike in the type locality. These limestones may correspond to temporary lakes or ponds that were formed in poorly-drained areas of mudflats, such as those reported by Bádenas et al. (2018) in the Tithonian–Berriasian record from the Galve Sub-basin (Fig. 1B). In the upper part of the interval (649.5–680 m), the clay deposits change upwards into channel-fill ostracod-rich limestones that mark the beginning of a long-term late Barremian–early Aptian transgression (Bover-Arnal et al. 2016). This interval represents the last non-marine deposits in the studied section.

The charophyte assemblage is very similar throughout the interval and strongly resembles that observed in Interval F. In this regard, *Atopochara trivolvis* var. *trivolvis*, *Clavator grovesii* var. *jiuquanensis*, and *C. harrisii* var. *harrisii* appear in this interval, but are absent in Interval F. *Porochara maestratica* is found in Interval F but is absent in interval H. *E. lazarii*, *A. trivolvis* var. *triquetra* and var. *trivolvis*, *C. harrisii* var. *reyi* and var. *harrisii* are abundant, well-preserved and occasionally attached to the thalli portions, suggesting autochthony. The utricles of *G. maillardii* var. *trochiliscoides* and var. *biutricularis*, *Clavator grovesii* var. *jiuquanensis*, *A. cruciata*, *H. neimongolensis* var. *neimongolensis*, *P. paucibracteatus*, and gyrogonites of aff. *M. harrisii* are less abundant and occasionally slightly abraded, indicating short lateral transport and parautochthony. Benthic foraminifera are abundant and well-preserved, indicating a marine influence, which is commonly described for mudflat settings (c.f. Bádenas et al. 2018).

5.2. The Fredes section

The Fredes section is exposed between kms 8 and 9 of the road CV-106 (Fig. 1D) and consists of a ~100 m-thick continuous Barremian succession that belongs entirely to the Cantaperdius Formation. It lies on the Herbers Formation, Hauterivian in age (e.g.,

466 Salas et al. 2001). The basal laterite of the Cantaperdius Formation consists of ~2.5 m of
467 yellowish and red clays that are topped by a mudstone limestone with root marks. The
468 charophyte assemblage in the laterite is mainly composed of *A. trivolvis* var. *triquetra*,
469 *A. stellata* var. *stellata*, *H. neimongolensis* var. *posticecaptus*, and gyrogonites of *P.*
470 *maestratica* and aff. *M. harrisii*. Thalli portions belonging to *Clavatoraxis* sp.,
471 *Favargerella aquavivae* and *Munieria grambastii* are rare, suggesting a
472 parautochthonous assemblage. Above the laterite, the section is divided into five
473 descriptive intervals A–E (Fig. 4). The laterite and the lower 10 m of the section are
474 repeated as the section is faulted.

475 **Interval A** (2.5–10.25 m and 13–26 m) is characterised by the occurrence of
476 lenticular limestone beds interbedded with marls. The marls form up to 1 m-thick beds
477 that are rich in charophyte thalli and fructifications, ostracods, molluscs and, frequently,
478 agglutinated benthic foraminifera, dasycladaleans, and vertebrate teeth. The limestones
479 are up to 3 m-thick (most commonly 1.5 m-thick). Their base is erosive and
480 characterised by lag deposits with a packstone texture containing molluscs, ostracods,
481 intraclasts, and rare charophyte thalli. Above the lag, the limestone is a mollusc-rich
482 wackestone-mudstone, forming a thinning-upwards sequence. Root marks as well as
483 nodular and intraclastic fabrics are observed at the top of the limestones.

484 The marls are interpreted as deposited in shallow lakes. The co-occurrence of
485 freshwater and brackish water organisms suggests that these lakes were probably
486 established in a coastal area that experienced alternating periods of freshwater and
487 marine influences. The overlying lenticular limestone beds are very similar to other
488 carbonate channel-fill deposits associated with lacustrine and palustrine areas (e.g., Platt
489 1989, Alonso-Zarza and Calvo 2000). The occurrence of intraclasts and the similarity of
490 the fossil contents of the limestones and the underlying marl intervals suggest the
491 reworking of the previously deposited shallow lake deposits during the sedimentation of

492 the channel-fill deposits. Nodular textures and root marks at the top of these lenticular
493 beds indicate the abandonment of the channel and the establishment of palustrine
494 conditions (see, e.g., Alonso-Zarza and Wright 2010).

495 The charophyte assemblage found in the marls is mainly composed of the utricles
496 of *A. trivolvis* var. *triquetra*, *A. stellata* var. *stellata* and var. *lata* (first occurrence), *A.*
497 *triquetra* and *H. neimongolensis* var. *posticecaptus*. These utricles are well-preserved
498 and frequently occur associated with or attached to thalli (*Clavatoraxis* sp., *F.*
499 *aquavivae* and *M. grambastii*), suggesting autochthony. On the other hand, *G.*
500 *maillardii* var. *trochiliscoides*, *C. harrisii* var. *dongjingensis*, *C. harrisii* var. *harrisii*,
501 aff. *M. harrisii* and *P. maestratica* are rare and frequently abraded, and found associated
502 with well-preserved dasycladalean and benthic foraminifera. This latter charophyte
503 assemblage is considered parauthocthonous in the sample.

504 **Interval B** (26–40.75 m) is formed of two different parts. The lower part (26−36
505 m) is characterised by decimetre-thick limestone beds, frequently showing vertical root
506 marks and nodular fabrics at the top, which are interbedded with thinner layers of marl,
507 all of them rich in charophyte thalli and fructifications as well as ostracods. The upper
508 part of the interval (35–40.75 m) starts with a thin marl bed containing abundant
509 charophyte remains (utricles, gyrogonites and thalli) together with abundant
510 agglutinated benthic foraminifera, molluscs and echinoid fragments. Above the marl
511 layer, the interval consists of repeating limestone parasequences composed of a basal
512 massive up to 2 m-thick wackestone that contains porocharacean gyrogonites, benthic
513 foraminifera, echinoid fragments, and rare clavatoracean remains, followed by a 0.2 m-
514 thick nodular limestone.

515 The lower part of the interval (26–35 m) is interpreted as a deposition in
516 freshwater shallow lakes that were later subaerially-exposed and, thus, the original rock
517 texture was modified by the establishment of palustrine conditions (see, e.g., Freytet

518 and Plaziat 1982, Alonso-Zarza and Wright 2010). The upper interval (35–40.75 m) was
519 probably deposited in coastal environments, with changing salinity and frequent
520 desiccation and emersion, as demonstrated by the presence of nodular limestones (see
521 similar examples in Alonso-Zarza and Wright 2010).

522 The charophyte assemblage identified in the marls of this interval resembles that
523 described in the previous interval, but with a slightly different preservation. The utricles
524 of *G. maillardii* var. *trochiliscoides* and, locally, *G. maillardii* var. *biutricularis* (first
525 occurrence) and *A. trivolvis* var. *triquetra* are abundant and well-preserved (indicating
526 autochthony), while those of *C. harrisii* var. *harrisii*, *A. stellata* var. *stellata* and var.
527 *lata*, *A. triquetra*, *H. neimongolensis* var. *posticecaptus*, aff. *M. harrisii* and *P.*
528 *maestratica* are scarce and can be abraded. The benthic foraminifera associated with the
529 charophytes are also abundant and well-preserved, suggesting a process of time
530 averaging between the deposition of the two different assemblages (freshwater and the
531 brackish to marine water, respectively).

532

533 ----------Please insert Fig. 4 near here----------

534

535 **Interval C** (40.75–71.5 m) is characterised by marl beds interbedded with
536 limestones. The marls are up to 2.5 m-thick and contain charophyte thalli and
537 fructifications (utricles and gyrogonites), ostracods, mollusc and echinoid fragments,
538 agglutinated benthic foraminifera, dasycladales and vertebrate teeth. The limestones are
539 0.25 to 1.5 m-thick and frequently display rootlet marks or nodular fabrics at the top.
540 There are three types of deposits: (1) massive clavatoracean-rich limestones containing
541 abundant clavatoracean utricles and thalli, ostracods, and molluscs, (2) massive
542 limestones rich in benthic foraminifera and fragments of molluscs, dasycladales, and
543 echinoids, and (3) lenticular cross-bedded bioclastic limestones with molluscs,

dasycladaleans, and benthic foraminifera that exhibit a basal lag deposit and become more fine upwards into a wackestone containing the same fossil content.

This interval is interpreted as coastal-marginal settings with alternating freshwater and brackish to marine water influences. Root marks and nodular fabrics observed at the top of some of the limestone beds indicate palustrine settings with subaerial exposition (e.g., Freytet and Plaziat 1982, Alonso-Zarza and Wright 2010). The lenticular cross-bedded bioclastic limestones observed at the top of the interval correspond to channel-fill deposits, probably formed in a coastal marine-influenced area.

The charophyte assemblages in this interval are mainly composed of well-preserved utricles of *G. maillardii* var. *trochiliscoides* (rarely *G. maillardii* var. *biutricularis*) and *A. trivolvis* var. *triquetra*. Occasionally, *E. lazarii* (first occurrence), *C. harrisii* var. *dongjingensis*, var. *harrisii*, and var *reyi* (first occurrence), *A. stellata* var. *stellata* (last occurrence), and var. *lata*, *A. triquetra* and *H. neimongolensis* var. *posticecaptus* (last occurrence) and var. *neimongolensis* (first occurrence), aff. *M. harrisii*, and *P. maestratica* do also occur. As in the underlying intervals A and B, samples with a higher abundance and better preservation of charophyte remains contain scarce, abraded and/or fragmented remains of marine organisms, while those with a higher abundance of marine organisms contain scarce and frequently abraded charophyte remains.

Interval D (71.5–88 m) is composed of thick limestone beds that are characterised by the frequent presence of oncoids and intraclasts. The marl layers interbedded with these limestones are very thin and contain charophyte thalli and fructifications, ostracods, molluscs and, occasionally, vertebrate teeth, dasycladales, and miliolids. The base of the interval (71.5–82 m) consists of two 5 m-thick parasequences, the bottom of which displays two up to 1 m-thick marl beds that are separated by a 0.5 m-thick charophyte-rich packstone limestone. Above this, each parasequence continues

with a 3 m-thick massive or laminated wackestone limestone containing large (~1 cm in diameter) black pebbles and oncoids. The upper part of Interval D (82–88 m) is distinguished by the occurrence of limestone beds with a massive fabric at the base that becomes nodular to brecciated at the top. These limestones are interbedded with thin layers of marl.

The whole interval is interpreted as a shallow lacustrine to palustrine succession. Black pebbles suggest more hydrodynamic lakeshore areas (e.g., Gierlowski-Kordesch 2010). The interbedding of nodular and brecciated limestones indicates palustrine facies (e.g., Alonso-Zarza and Wright 2010), while the massive limestones correspond to well-oxygenated lacustrine deposits (e.g., Gierlowski-Kordesch 2010). The absence or scarcity of remains from marine organisms indicates a deposition in freshwater settings.

The charophyte assemblage in this interval is mainly formed of well-preserved *A. trivolvis* var. *triquetra* and, occasionally, superficially eroded specimens of *G. maillardii* var. *trochiliscoides* and var. *biutricularis*, *A. stellata* var. *lata*, *A. triquetra*, *H. neimongolensis* var. *neimongolensis*, aff. *M. harrisii* and *P. maestratica*. *E. lazarii* is rare, but showing complete fertile whorls. In the uppermost part of the interval (82–88 m), charophyte biodiversity increases and the assemblages are composed of well-preserved fructifications of the aforementioned taxa together with those of *Clavator grovesii* var. *gautieri* and *C. harrisii* var. *reyi* that are associated with thalli (*F. aquavivae*, *Clavatoraxis* sp., and *Charaxis* aff. *spicatus*), sometimes in anatomical connection, indicating an autochthonous assemblage.

----------Please insert Fig. 5 near here----------

Interval E (88–98 m) is dominated by massive (locally nodular) clavatoracean-rich marl beds that are up to 1.7 m-thick and contain ostracods, and molluscs. These are

interbedded with up to 1 m-thick limestones. Based on textures and fossils, two microfacies can be distinguished: (1) oyster-rich grainstones that also contain gastropods and benthic foraminifera, and (2) wackestone limestones rich in porocharacean gyrogonites that also contain less-abundant molluscs and benthic foraminifera. The whole interval is interpreted as coastal shallow lakes, laterally-associated with brackish water and marine environments.

This interval contains richer charophyte assemblages than those observed in the underlying interval, including *E. lazarii*, *G. maillardii* var. *trochiliscoides*, and var. *biutricularis*, *A. trivolvis* var. *triquetra*, *C. grovesii* var. *gauteri*, *C. harrisii* var. *dongjingensis* (last occurrence), var. *harrisii*, and var. *reyi*, *Clavator calcitrapus* var. *jiangluoensis*, and var. *calcitrapus* (first occurrence), *A. stellata* var. *lata*, *A. triquetra*, *H. neimongolensis* var. *neimongolensis*, and rarely also *P. maestratica* and aff. *M. harrsii*. The utricles and gyrogonites are generally well-preserved and associated with charophyte thalli (*Charaxis* sp., *Clavatoraxis* sp., *F. aquavivae*, and *M. grambastii*), suggesting autochthony of the charophyte assemblage.

6. Strontium-Isotope Stratigraphy (SIS)

6.1. Preservation of the original $^{87}Sr/^{86}Sr$ signature

Evaluation of the preservation state of low-Mg calcite shells is a primary requirement in SIS. Diagenetic processes during burial may modify the original $^{87}Sr/^{86}Sr$ ratio, resulting in an erroneous derivation of the age. The analysis of major and trace elements is an effective tool to evaluate any changes in biogenic samples (e.g., Steuber et al. 2005, Bodin et al. 2009, Huck et al. 2011, Frijia et al. 2015, Bover-Arnal et al. 2016, Caus et al, 2016, González-León et al. 2017). Diagenetic alterations in biogenic samples commonly result in a decrease in Sr concentration and an increase in Fe and Mn concentrations as well as in the $^{87}Sr/^{86}Sr$ ratio (Brand and Veizer 1980,

622 Wenzel 2000). However, these trends were not observed in our results, which are
623 summarised in Table 2. Except for sample OyFr1, which is clearly altered due to
624 diagenesis, the Sr concentrations are >700 ppm (Table 2). A Sr concentration > 700
625 ppm is usually considered a minimum value for discriminating between non-
626 diagenetically-altered samples and diagenetically-altered samples (e.g., Boix et al.,
627 2011; Frijia et al., 2015). Moreover, in most samples, the Mn and Fe concentrations are
628 above the threshold values (50 ppm and 250 ppm, respectively) that discern between
629 diagenetically-altered and non-diagenetically-altered samples (e.g., Steuber 1999,
630 2001). However, high Fe and Mn concentrations have also been linked to sedimentary
631 processes. Schneider et al. (2009) indicated that in marginal marine conditions, Fe and
632 Mn concentrations can be affected by freshwater influx and suggested cut-off values of
633 Mn <250 ppm and Fe <700 ppm for oysters found in such settings. On the other hand,
634 low Mn and Fe concentrations can also occur in diagenetic calcite (Steuber et al. 2005,
635 Boix et al. 2011, Frijia et al. 2015, Bover-Arnal et al. 2016, Caus et al. 2016).
636 Therefore, low Mn and Fe concentrations and high Sr concentrations have to be used
637 cautiously as indicators of non-diagenetic overprint of biogenic low-Mg calcite.
638 In our dataset, 6 out of the 10 samples (OyFr2, OyFr21c, OyH3, OyH4, OyH6,
639 and OyH7; Table 2) have Mn and Fe concentrations that are below the threshold values
640 (Mn < 250 ppm and Fe < 700 ppm) distinguishing between diagenetically-altered and
641 non-diagenetically-altered oyster shells from marginal marine environments (e.g.,
642 Schneider et al., 2009; Horikx et al., 2014). Following Brasier et al. (1994), Denison et
643 al. (1994) and Rosales et al. (2001), we used the Mn/Sr and Fe/Sr ratios to discern
644 between diagenetically-altered and non-diagenetically-modified samples (Table 2).
645 Ratios of Mn/Sr <0.5 and Fe/Sr <0.3 were proposed by Brasier et al. (1994) to
646 distinguish between altered and non-altered carbonates. Based on this criterion, only

three samples, OyFr21c, OyH4 and OyH6 (Table 2), preserved non-altered $^{87}Sr/^{86}Sr$ values and were finally used to derive the numerical ages.

The discarded samples OyH3 and OyH7 show Sr-isotope ratios of 0.707515 and 0.707504, respectively, which are not in agreement with the marine $^{87}Sr/^{86}Sr$ ratios published for the Barremian Stage. According to McArthur et al. (2012), the Barremian Sr-isotope values range between 0.707471 and 0.707432, whereas McArthur et al. (2020) give a range between 0.707470 and 0.707426. The oyster shells OyFr2, OyH3 and OyH7 discarded were collected from beds that contain abundant and well-preserved charophytes (Figs. 3B and 4). Therefore, the isotopic signal of these samples was probably modified by freshwater influence (see e.g., Benito et al. 2020; Table 2).

6.2. Strontium ratios and the derived numerical ages

Non-diagenetically-altered samples used for SIS were collected from the Cantaperdius Formation (sample OyFr21c) and the Artoles Formation (samples OyH4 and OyH6) (Figs. 3A-B and 4; Table 2). The $^{87}Sr/^{86}Sr$ ratios obtained from the low-Mg calcite oyster shells from these units vary from 0.707481 ± 0.000012 to 0.707489 ± 0.000012 (Table 2). Taking into account the stratigraphic context, these values were converted into numerical ages using the 'LOWESS 5 fit 26 03 13' look-up table of McArthur, which is linked to the Geologic Time Scale 2012 (GTS2012) of Gradstein et al. (2012), and the 'LOESS 6 16 03 2020' look-up table of McArthur (J. McArthur, personal communication, 2021), which is linked to the Geologic Time Scale 2020 (GTS2020) of Gradstein et al. (2020). In both Geologic Time Scales, the whole-time range of the samples is latest Hauterivian–late Barremian (Table 2). The reason why these $^{87}Sr/^{86}Sr$ values translate into such a wide time span is due to the slow increase in the $^{87}Sr/^{86}Sr$ ratios between the early Barremian and the early late Barremian (see, e.g., Jones and Jenkins 2001, McArthur et al. 2001, 2012, 2020, Mutterlose et al. 2014, Wan

673 et al. 2019). However, the data available on charophyte biostratigraphy at the base of
674 the studied sections constrains the age of these samples to the Barremian (e.g., Martín-
675 Closas and Salas 1994, Martín-Closas 2000).

676 According to the numerical ages derived from the 'LOWESS 5 fit 26 03 13' look-
677 up table of McArthur, which is linked to the GTS2012, the $^{87}Sr/^{86}Sr$ ratios indicate
678 preferred ages of between 129.80 and 129.00 Ma, dating the analysed specimens to the
679 early Barremian–early late Barremian. Considering the statistical uncertainty (2 s.e.),
680 the total age range for the samples is 130.95–128.25 Ma (latest Hauterivian–late
681 Barremian; Ogg and Hinnov, 2012).

682 The oldest low-Mg calcite sample was obtained from the Cantaperdius Formation
683 in the Fredes section (sample OyFr21c; Fig. 4). The $^{87}Sr/^{86}Sr$ ratio of this sample is
684 0.707481 ± 0.000012, translating into a preferred numerical age of 129.80 Ma (+1.15/-
685 0.60). This numerical age corresponds to the late early Barremian (Ogg and Hinnov,
686 2012). The two other analysed samples were obtained from the Herbers-Mas de Petxí
687 section (Fig. 3A–B). Sample OyH4 was obtained from the lower part of the Artoles
688 Formation and its $^{87}Sr/^{86}Sr$ ratio is 0.707482 ± 0.000012, which translates into a
689 preferred age of 129.70 Ma (+1.20/-0.60), i.e., early Barremian (Ogg and Hinnov,
690 2012). The youngest low-Mg calcite shell sample was OyH6, which was obtained from
691 the topmost part of the Artoles Formation, specifically, 1.5 m below the second interval
692 of the Morella Formation in the Herbers-Mas de Petxí section (Fig. 3B). The $^{87}Sr/^{86}Sr$
693 value for this sample is 0.707489 ± 0.000012, which translates into a preferred age of
694 129.00 Ma (+0.80/-0.75), corresponding to the early late Barremian (Ogg and Hinnov,
695 2012).

696 On the other hand, utilizing the 'LOESS 6 16 03 2020' look-up table of
697 McArthur, which is associated to the GTS2020, the preferred numerical ages fall within
698 the early Barremian and range between 126.10 and 125.05 Ma (Table 2). Taking into

account the statistical uncertainty, however, the total time span for the sample is 126.65–124.20 Ma (latest Hauterivian–early late Barremian according to Gale et al. 2020). However, this recent numerical calibration shows inconsistencies. For example, according to the 'LOESS 6 16 03 2020', the preferred numerical age derived for sample OyH6 is 125.05 Ma (Table 2) and falls within the early early Barremian. Sample OyH6 is 24 m below the first appearance of *Clavator grovesii* var. *jiuquanensis* (Fig. 3B), which has been correlated with the *Toxanclyoceras vandenheckii* ammonoid biozone (late Barremian) in the Subalpine Chains (Martín-Closas et al. 2009). According to Gale et al. (2020), the base and top of the *Toxanclyoceras vandenheckii* Zone is dated to 124.4 and 123 Ma, respectively. This would imply that the 24 m of stratigraphic succession found between sample OyH6 and the the first occurrence of *Clavator grovesii* var. *jiuquanensis* (Fig. 3B) would record 0.65 My. Such a significant sedimentary gap or slow rate of sedimentation seems unlikely given the overall expansion and large thickness of the synrift succession studied (Fig. 3A-B). In consequence, the biozonations presented herein follow the GTS2012, which provides a more consistent chrono-biostratigraphic framework (Fig. 6), and is in agreement with previous correlations between charophyte assemblages and ammonoid biostratigraphy (Martín-Closas et al. 2009).

----------Please insert Table 2 near here----------

7. Barremian-early Aptian charophyte biozonation

The new data obtained from the two Barremian sections studied enabled us to refine the Barremian-early Aptian European charophyte biozonation and extend its use to most of the Cretaceous Tethyan Archipelago (mainly present-day Europe and North Africa). Moreover, the new data led us to propose a new Barremian-early Aptian

Eurasian charophyte biozonation, whose index species were widely distributed from Europe to China. The two biozonations are directly correlated to one another in Figures 3A–B, 4 and 6.

7.1. The Barremian–early Aptian European charophyte biozonation

The first proposal of a Barremian-early Aptian European charophyte biozonation was from Grambast (1974) and was later modified by Martín-Closas and Salas (1994), Riveline et al. (1996), and finally by Martín-Closas et al. (2009). The current biozonation (after the revision of Martín-Closas et al., 2009) is composed of two partial range biozones that are characterised at their bases by the FAD of *Atopochara trivolvis* var. *triquetra* (early Barremian) and *Ascidiella cruciata* and *Pseudoglobator paucibracteatus* (late Barremian-early Aptian; Fig. 6), respectively. Herein, we propose to modify this biozonation by only using species that are known to have been endemic in the Cretaceous Tethyan Archipelago. Following this criterion, *Globator maillardii* var. *trochiliscoides* is proposed here as the index species of the early Barremian charophyte biozone instead of *A. trivolvis* var. *triquetra*. This new index species was extensively distributed and appears to have been endemic in Europe and most of the Cretaceous Tethyan Archipelago (Martín-Closas, 2000; Martín-Closas and Wang 2010; Pérez-Cano et al., 2020; Sanjuan et al. 2021), while *A. trivolvis* var. *triquetra*, which had a cosmopolitan distribution during the Barremian (Martín-Closas and Wang, 2008), is reserved for the Eurasian biozonation (see below). By contrast, the late Barremian–early Aptian Ascidiella cruciata-Pseudoglobator paucibracteatus biozone is kept unchanged in the new proposal (Fig. 6), since these index species are, so far, unique to the Cretaceous Tethyan Archipelago.

Globator maillardii var. trochiliscoides biozone

751 **Definition.** Partial range biozone defining the interval between the FAD of
752 *Globator maillardii* var. *trochiliscoides* and the FAD of *Ascidiella cruciata* and
753 *Pseudoglobator paucibracteatus* (Figs. 3A–B and 6).
754 **Species assemblage:** *Echinochara lazarii*, *Globator mallardii* var. *trochiliscoides*
755 (dominant over *G. maillardii* var. *biutricularis*), *G. maillardii* var. *biutricularis*,
756 *Atopochara trivolvis* var. *triquetra*, *Clavator grovesii* var. *gautieri*, *C. harrisii* var.
757 *dongjingensis*, *C. harrisii* var. *harrisii* (dominant over var. *dongjingensis* and var. *reyi*),
758 *C. harrisii* var. *reyi*, *C. calcitrapus* var. *jiangluoensis*, *C. calcitrapus* var. *calcitrapus*,
759 *Ascidiella stellata* var. *stellata*, *A. stellata* var. *lata* (dominant over var. *stellata*), *A.*
760 *triquetra*, *A. iberica* var. *iberica*, *Hemiclavator adnatus*, *H. neimongolensis* var.
761 *posticecaptus*, *H. neimongolensis* var. *neimongolensis*, and *Pseudoglobator fourcadei*.
762 **Remarks.** A biozone based on *G. maillardii* var. *trochiliscoides* was previously
763 proposed by Mojon (1996) to characterise the late Barremian–early Aptian. The same
764 author proposed the G. maillardii var. mutabilis biozone for the lower Barremian.
765 However, the populations of *G. maillardii* observed in the oldest assemblages studied
766 herein (in the lower part of the Cantaperdius Formation) do not show the basal utricle
767 features characteristic of *G. maillardii* var. *mutabilis* (cf. Martín-Closas 2000), fully
768 belonging to var. *trochiliscoides* instead. This criterion of homogeneous populations of
769 *G. maillardii* var. *trochiliscoides* was used to establish the base of the G. maillardii var.
770 trochiliscoides biozone. However, some utricles (<10%) of *G. maillardii* var.
771 *biutricularis* may occur in particular *G. maillardii* var. *trochiliscoides* populations of
772 this biozone, while *G. maillardii* var. *biutricularis* can be more frequent than *G.*
773 *maillardii* var. *trochiliscoides* or even dominant in the overlying Ascidiella cruciata-
774 Pseudoglobator paucibracteatus biozone, where it can form homogeneous populations
775 (e.g., Vicente and Martín-Closas 2013).

776 The *C. harrisii* populations in the G. maillardii var. trochiliscoides biozone are
777 dominated by *C. harrisii* var. *harrisii*, which is the typical variety in this biozone and
778 frequently forms homogeneous populations (Martín-Closas 2000 and references
779 therein). However, some utricles of *C. harrisii* var. *dongjingensis* and *C. harrisii* var.
780 *reyi* are repeatedly found in the studied samples to be in association with *C. harrisii* var.
781 *harrisii*. *C. harrisii* var. *dongjingensis* was typical and dominant between the late
782 Berriasian and late Hauterivian (Martín-Closas 2000). *C. harrisii* var. *reyi* occurs for the
783 first time in this biozone inside populations dominated by *C. harrisii* var. *harrisii*.
784 However, *C. harrisii* var. *reyi* is typical and dominant in the overlying Cruciata-
785 Paucibracteatus biozone, where it forms homogeneous populations (e.g., Vicente and
786 Martín-Closas 2013).
787 *C. calcitrapus* var. *jiangluoensis* occurs in the lower part of the G. maillardii var.
788 trochiliscoides biozone, while *C. calcitrapus* s.s. occurs in the upper part of the biozone.
789 Therefore, the gradualistic evolution of *C. calcitrapus* described by Pérez-Cano et al.
790 (2020) allows more precise dating throughout this biozone.
791 Two more species are also characteristic of this biozone, although they have not
792 been identified in the stratigraphic sections studied here. These are *Ascidiella iberica*
793 var. *iberica* (Grambast) Martín-Closas ex Schudack, which occurs in association with *A.*
794 *trivolvis* var. *triquetra* in several localities of the Iberian Chain in Spain and in the
795 Wealden Basin in England (Martín-Closas 2000 and Feist et al. 1995, respectively), and
796 *Pseudoglobator fourcadei* Grambast, which has been exclusively described in the
797 Prebaetic Chain (south-eastern Spain), where it occurs in association with *A. trivolvis*
798 var. *triquetra* and *H. adnatus* (Martín-Closas 2000).
799 **Biostratigraphic correlations.** In the Iberian Chain, *G. maillardii* var.
800 *trochiliscoides* has been correlated with the orbitolinid foraminifer *Palaeodictyoconus*
801 *cuvillieri* (Combes et al., 1966). In the Subalpine Chains, *G. maillardii* var.

trochiliscoides has been correlated with the orbitolinid assemblage composed of *Valserina broennimanni*, *Eopalorbitolina charollaisi*, *Orbitolinopsis debelmasi*, *Cribellopsis elongata* and *Paracoskinolina hispanica*, corresponding to the *Nicklesia nicklesi* ammonite Zone (Martín-Closas et al. 2009).

Calibration based on SIS. No calibration is available for the base of the biozone, while its top coincides with the base of the next biozone, which is calibrated as explained below.

Age. Early Barremian.

Ascidiella cruciata-Pseudoglobator paucibracteatus biozone

Definition. Time interval defined between the FAD of *Ascidiella cruciata* and *Pseudoglobator paucibracteatus*, and the FAD of *Clavator grovesii* var. *lusitanicus*.

Species assemblage. *Echinochara lazarii*, *Globator mallardi* var. *trochiliscoides*, *G. maillardii* var. *biutricularis* (dominant over var. *trochiliscoides*), *Atopochara trivolvis* var. *triquetra* (dominant variety upon var. *trivolvis*), *Atopochara trivolvis* var. *trivolvis*, *Clavator grovesii* var. *gautieri*, *C. grovesii* var. *jiuquanensis*, *C. harrisii* var. *harrisii*, *C. harrisii* var. *reyi* (dominant over var. *harrisii*), *Hemiclavator neimongolensis* var. *neimongolensis, Ascidiella cruciata, A. iberica* var. *inflata* and *Pseudoglobator paucibracteatus.*

Remarks. Riveline et al. (1996) defined this biozone as a partial range biozone described between the FAD of *A. cruciata* and the FAD of *C. grovesii* var. *lusitanicus*. Later, Martín-Closas et al. (2009) redefined this biozone as a total range biozone limited between the FAD of *A. cruciata* and *P. paucibracteatus* and the last appearance datum (LAD) of *P. paucibracteatus*. The redefinition as a partial range biozone in this paper follows the original characterisation of the late Barremian Ascidiella cruciata partial range biozone of Riveline et al. (1996) but using the FAD of *A. cruciata* and *P.*

828 *paucibracteatus*. This avoids possible problems of (1) overlapping between the
829 Ascidiella cruciata-Pseudoglobator paucibracteatus biozone and the overlying Clavator
830 grovesii var. lusitanicus biozone if the LAD of *P. paucibracteatus* is found to be
831 younger than the FAD of *C. grovesii* var. *lusitanicus* and (2) occurrence of an undefined
832 interval between the two biozones. Such poorly defined biostratigraphic intervals are
833 usually designed as interval biozones.

834 *A. trivolvis* var. *trivolvis* occurs in this biozone. However, it never forms
835 homogeneous populations but it is found associated with *A. trivolvis* var. *triquetra*,
836 which is the dominant variety in the Cruciata-Paucibracteatus biozone. Homogeneous
837 populations of *A. trivolvis* var. *trivolvis* are typical of the overlying Clavator grovesii
838 var. corrugatus biozone (Riveline et al. 1996). *Ascidiella iberica* var. *inflata* (Grambast-
839 Fessard) Martín-Closas has not been identified in the studied sections. However,
840 Martín-Closas (2000) reported it from beds interbedded with *Palorbitolina lenticularis*
841 in other sections from the Maestrat basin.

842 **Biostratigraphic correlations.** In the Subalpine Chains, *P. paucibracteatus* has
843 been observed in a marl level above a grainstone bed containing *Paleodictyoconus*
844 *cuvillieri*, *Paleodictyoconus actinostoma* and *Cribrellopsis neoelongata* (Mojon, 1988).
845 Martín-Closas et al. (2009) found *P. paucibracteatus* in marl beds interbedded with
846 marine layers alongside an orbitolinid assemblage composed of *Orbitolinopsis kiliani*,
847 *O. cuvillieri*, *O. buccifer* and *Palorbitolina lenticularis*. These authors correlated this
848 assemblage with the Barremian ammonite biozones of *Toxancyloceras vandenheckii*,
849 *Gerhardtia sartousiana*, *Hemihoplites feraudianus* (now the upper subzone of
850 *Gerhardtia sartousiana* according to Reboulet et al. 2018), *Imerites giraudi* and
851 *Martelites sarasini*. In the Iberian Chain, *A. cruciata* has been repeatedly correlated
852 with *P. lenticularis* (Martín-Closas, 2000 and references therein).

853 **Calibration based on SIS.** In the Herbers-Mas de Petxí section, the FAD of *P.*
854 *paucibracteatus* occurs in a marl bed at the basal part of the Artoles Formation (sample
855 H124; Fig. 3B), which is located 5 m below the stratigraphic layer where sample OyH4
856 was collected (Fig. 3B). An $^{87}Sr/^{86}Sr$ ratio of 0.707482 ± 0.000012 was obtained for this
857 oyster shell, translating into a preferred age of *c*. 129.70 Ma (+1.20/-0.50) (Table 2) for
858 the base of this biozone. No calibration is available yet for the top of the biozone.
859 **Age.** Late early Barremian–early Aptian.
860
861 **7.2. The Barremian-early Aptian Eurasian charophyte biozonation**
862 **Atopochara trivolvis var. triquetra biozone**
863 **Definition.** Time interval defined between the FAD of *Atopochara trivolvis* var.
864 *triquetra* and the FAD of *Hemiclavator neimongolensis* var. *neimongolensis*.
865 **Species assemblage (Family Clavatoraceae) in the basins of the Cretaceous**
866 **Tethyan Archipelago.** *Echinochara lazarii*, *Globator mallardii* var. *trochiliscoides*
867 (dominant over *G. maillardii* var. *biutricularis*), *G. maillardii* var. *biutricularis*,
868 *Clavator grovesii* var. *gautieri*, *Ascidiella stellata* var. *stellata*, *A. stellata* var. *lata*
869 (dominant over *A. stellata* s.s.), *A. triquetra*, *A. iberica* var. *iberica*, *Hemiclavator*
870 *adnatus*, *H. neimongolensis* var. *posticecaptus*, and *Pseudoglobator fourcadei*.
871 **Species assemblage (Family Clavatoraceae) in all the Eurasian basins.**
872 *Atopochara trivolvis* var. *triquetra*, *Clavator harrisi* var. *dongjingensis*, *C. harrisii* var.
873 *harrisii* (dominant over var. *dongjingensis* and var. *reyi*) and *C. calcitrapus* var.
874 *jianglouensis*.
875 **Remarks.** Riveline et al. (1996) characterised it as a partial range biozone that
876 was defined between the FAD of *A. trivolvis* var. *triquetra* and the FAD of *Ascidiella*
877 *cruciata* in the European biozonation. Due to the cosmopolitan distribution of *A.*
878 *trivolvis* var. *triquetra* (Martín-Closas and Wang 2008), this biozone is redefined herein

879 as a Eurasian biozone, with its upper boundary modified to the FAD of *H.*
880 *neimongolensis* var. *neimongolensis*.
881 The FAD of *A. trivolvis* var. *triquetra* seems to occur at least in the late
882 Hauterivian, where it appeared to be associated with *A. trivolvis* var. *ancora* (Fig. 3A).
883 However, it is not until the base of the Barremian when *A. trivolvis* var. *triquetra*
884 formed homogenous populations. This criterion, i.e., the occurrence of homogeneous
885 populations of this anagenetic variety, was used here to define the base of the *A.*
886 *trivolvis* var. *triquetra* biozone.
887 **Biostratigraphic correlations.** *A. trivolvis* var. *triquetra* frequently appears with
888 *G. maillardii* var. *trochiliscoides* in the Iberian Chain (e.g., Combes et al. 1966, Martín-
889 Closas and Salas 1994, Martín-Closas 2000) and in the Subalpine Chains (Martín-
890 Closas et al. 2009). Thus, it has been correlated with the same orbitolinid species and
891 ammonite biozones as those for the *G. maillardii* var. *trochiliscoides* biozone.
892 **Calibration based on SIS**. The upper boundary of this biozone was calibrated in
893 the Fredes section with an $^{87}Sr/^{86}Sr$ ratio obtained from a low-Mg oyster shell belonging
894 to sample OyFr21c (Fig. 4 and Table 2). The $^{87}Sr/^{86}Sr$ value is 0.707481 ± 0.000012,
895 translating into a preferred numerical age of 129.80 Ma (+1.15/-0.60).
896 **Age.** Early Barremian.
897
898 **Hemiclavator neimongolensis var. neimongolensis biozone**
899 **Definition**. Partial range biozone defining the interval between the FAD of
900 *Hemiclavator neimongolensis* var. *neimongolensis* and the FAD of *Clavator grovesii*
901 var. *jiuquanensis.*
902 **Species assemblage (Family Clavatoraceae) in the basins of the Cretaceous**
903 **Tethyan Archipelago.** *Echinochara lazarii*, *Globator mallardi* var. *trochiliscoides*, *G.*
904 *maillardii* var. *biutricularis*, *Clavator grovesii* var. *combei, C. calcitrapus* var.

905 *calcitrapus*, *Ascidiella stellata* var. *lata, A. triquetra*, *A. cruciata*, *A. iberica* var. *inflata*,
906 and *Pseudoglobator paucibracteatus.*

907 **Species assemblage (Family Clavatoraceae) in all the Eurasian basins.**
908 *Atopochara trivolvis* var. *triquetra, Clavator harrisii* var. *dongjingensis, C. harrisii* var.
909 *harrisii* (dominant variety of this species)*, C. harrisii* var. *reyi, C. calcitrapus* var.
910 *jiangluoensis*, and *Hemiclavator neimongolensis* var. *neimongolensis*.

911 **Remarks.** The base of the biozone is marked by the first homogeneous population
912 of *H. neimongolensis* var. *neimongolensis*. In the Herbers-Mas de Petxí section, mixed
913 populations of *H. neimongolensis* var. *posticecaptus* and *H. neimongolensis* var.
914 *neimongolensis* occur in the uppermost part of the *A. trivolvis* var. *triquetra* biozone
915 (e.g., samples H36–H38; Fig 3A), while the first homogeneous population of *H.*
916 *neimongolensis* var. *neimongolensis* occurs a few metres above (sample H39; Fig 3A).
917 The wide biogeographic range of *H. neimongolensis* var. *neimongolensis* and its quick
918 expansion from Iberia to China (Martín-Closas 2015) make this species a useful tool to
919 perform intercontinental correlations of non-marine successions.

920 Homogeneous populations of *C. calcitrapus* var. *jiangluoensis* can be found at the
921 base of the Hemiclavator neimongolensis var. neimongolensis biozone, while
922 homogenous populations of *C. calcitrapus* s.s. are found only in the upper part of the
923 biozone. In fact, the *C. calcitrapus* populations observed in the H. neimongolensis var.
924 neimongolensis biozone frequently contain both *C. calcitrapus* var. *jiangluoensis* and *C.*
925 *calcitrapus* s.s., as well as intermediate morphotypes.

926 **Calibration based on SIS.** The FAD of the index species in the Fredes section
927 occurs in sample Fr21c (Fig. 4) in association with oyster shells (sample OyFr21c;
928 Table 2). The $^{87}Sr/^{86}Sr$ value obtained for this sample is 0.707481 ± 0.000012, which
929 gives a preferred age of 129.80 Ma (+1.15/-0.60).

930 **Age.** Late early Barremian–early late Barremian.

931

932 **Clavator grovesii var. jiuquanensis biozone**

933 **Definition.** Partial range biozone comprising the interval between the FAD of
934 *Clavator grovesii* var. *jiuquanensis* and the FAD of *Clavator grovesii* var. *corrugatus*.

935 **Species assemblage (Family Clavatoraceae) in the basins of the Cretaceous**
936 **Tethyan Archipelago.** *Echinochara lazarii*, *Globator maillardii* var. *trochiliscoides*, *G.*
937 *maillardii* var. *biutricularis* (dominant over var. *trochiliscoides*), *Ascidiella cruciata*, *A.*
938 *iberica* var. *inflata*, and *Pseudoglobator paucibracteatus.*

939 **Species assemblage (Family Clavatoraceae) in all the Eurasian basins.**
940 *Atopochara trivolvis* var. *triquetra* (dominant over var. *trivolvis*), *A. trivolvis* var.
941 *trivolvis, Clavator grovesii* var. *jiuquanensis, Clavator harrisii* var. *harrisii*, *C. harrisii*
942 var. *reyi* (dominant over var. *harrisii*), and *Hemiclavator neimongolensis* var.
943 *neimongolensis*.

944 **Remarks.** *C. grovesii* var. *jiuquanensis* was used by Wang and Lu (1982) to
945 define the Perimneste ancora–Clypeator jiuquanensis assemblage biozone (former
946 taxonomy for *Atopochara trivolvis* var. *ancora* and *C. grovesii* var. *jiuquanensis*,
947 respectively) with a Hauterivian-lower Barremian age range in the Chinese basins.
948 Similar ages were suggested for the Mesochara stipitata-Clypeator jiuquanensis-
949 Flabellochara hebeiensis assemblage biozone (the latter a synonym of *C. harrisii* var.
950 *harrisii*) defined by Peng et al. (2003). Yang et al. (2008) proposed a Clypeator
951 jiuquanensis biozone that characterized the Hauterivian and the Barremian. However,
952 recent data about the age of this taxon in China also suggest a late Barremian-early
953 Aptian age (Li et al. 2020), similar to the ages observed in Europe.

954 The Clavator grovesii var. jiuquanensis biozone comprises most of the
955 biostratigraphic interval of the European Cruciata-Paucibracteatus biozone of Martín-
956 Closas et al. (2009). However, the Eurasian biogeographic range of *C. grovesii* var.

957 *jiuquanensis* and its quick spread throughout the entire Eurasian domain (Martín-Closas
958 2015) favours its use as a valuable index species to perform non-marine intercontinental
959 correlations with.

960 **Biostratigraphic correlations.** In the Subalpine Chains, *C. grovesii* var.
961 *jiuquanensis* occurs together with *P. paucibracteatus* (Martín-Closas et al. 2009),
962 indicating that the *C. grovesii* var. *jiuquanensis* biozone can be correlated with benthic
963 foraminifera and ammonite biozones similar to those used for the Cruciata-
964 Paucibracteatus biozone.

965 **Calibration based on SIS.** The FAD of the index species is 24.5 m above the
966 oyster bed from where sample OyH6 was collected in the Herbers-Mas de Petxí section
967 (Fig. 3B). The $^{87}Sr/^{86}Sr$ of 0.707489 ± 0.000012 obtained with this sample translates
968 into a preferred age of 129 Ma (+0.80/-0.75).

969 **Age.** Late Barremian–early Aptian.

970

971 ----------Please insert Fig. 6 near here----------

972

973 **8. Discussion**

974 **8.1. The Barremian-early Aptian charophyte biozonation revisited**

975 Two different Barremian–early Aptian charophyte biozonations, one for the
976 Cretaceous Tethyan Archipelago (European) and the other for the whole Eurasian
977 domain, are proposed herein (Fig. 6). The European biozonation is formed of index
978 species that are exclusive to Europe and North Africa, whereas the Eurasian biozonation
979 is composed of sub-cosmopolitan to cosmopolitan index species based on the
980 biogeographic studies of Martín-Closas and Wang (2008) and Martín-Closas (2015).

981 The new Barremian Eurasian biozonation proposed in this paper is composed of
982 three biozones that characterise (1) the early Barremian (the Atopochara trivolvis var.

triquetra biozone), (2) the late early Barremian–early late Barremian (the Hemiclavator neimongolensis var. neimongolensis biozone) and (3) the late Barremian–early Aptian (the Clavator grovesii var. jiuquanensis biozone), respectively. This provides a better biostratigraphic resolution than the European and Chinese charophyte biozonations used to date (e.g., Riveline et al. 1996, Martín-Closas et al. 2009 and Wang and Lu 1982, Yang et al. 2008, respectively). This is surprising since high-resolution charophyte biozonations are often regional, basin-wide to continent-limited (e.g., Sanjuan et al. 2014, Vicente et al. 2015, 2016 for Europe with regional subzones; Li et al. 2019 for North China), while sub-cosmopolitan to cosmopolitan species usually usually have lower evolutionary rates, resulting in less precise biostratigraphic subdivisions. For instance, Li et al. (2016) proposed a late Campanian–late Maastrichtian Eurasian Microchara cristata biozone, which was later considered a superzone and subdivided into three regional Chinese biozones (Li et al. 2019).

The Eurasian A. trivolvis var. triquetra biozone is equivalent to the biozone with the same index species described by Riveline et al. (1996) and Martín-Closas et al. (2009), except that its upper boundary has been modified to the FAD of *H. neimongolensis* var. *neimongolensis*. The H. neimongolensis var. neimongolensis biozone was originally proposed as a regional Iberian subzone for the upper part of the Atopochara trivolvis var. triquetra biozone by Martín-Closas and Salas (1994) and Martín-Closas and Schudack in Riveline et al. (1996). This subzone was first used to resolve biostratigraphic correlations within Iberia (Martín-Closas and Alonso-Millán 1998), since the index species was unknown in other European basins. Later, it was reported to be present in the Subalpine Chains and Jura Mountains in France and Switzerland (Martín-Closas et al. 2009). It was already known to occur in China (Wang and Lu 1982).

1008 The Hemiclavator neimongolensis var. neimongolensis biozone directly correlates
1009 with the upper part of the Globator maillardii var. trochiliscoides European biozone and
1010 the base of the Ascidiella cruciata-Pseudoglobator paucibracteatus European biozone
1011 (Fig. 6), indicating that the charophyte assemblage of this biozone is composed of
1012 species from both European biozones (sections 7.1 and 7.2).
1013 *Clavator grovesii* var. *jiuquanensis* is the index species of the third Eurasian
1014 biozone (late Barremian–early Aptian). This species was previously used as an index
1015 species to characterise a Hauterivian–early Barremian biozone in Chinese basins (Wang
1016 and Lu 1982, Peng et al. 2003, Yang et al. 2008). However, more recent data from the
1017 Jiuquan Basin suggest a late Barremian–early Aptian (more probably early Aptian) age
1018 for this species (Li et al. 2020), based on a previous chemostratigraphic ($\delta^{13}C$ and $\delta^{18}O$)
1019 study performed by Suárez et al. (2013) and through comparisons with the age of *C.*
1020 *grovesii* var. *jiuquanensis* given by Martín-Closas et al. (2009) in Europe. The derived
1021 numerical ages obtained in the present study agree with the ages previously suggested
1022 for *C. grovesii* var. *jiuquanensis* in Eurasia.
1023
1024 **8.2. Comparison with other Barremian charophyte biozonations**
1025 The European Barremian biozonations proposed to date followed and modified
1026 the pioneering proposal by Grambast (1974), who defined two assemblage biozones, 'El
1027 Mangraner' (early Barremian) and 'San Carlos' (late Barremian), which were obtained
1028 after studying the clavatoracean succession in the Eastern Iberian Chain. These biozones
1029 were the base for the European or more local charophyte biozonations, such as those by
1030 Feist et al. (1995) and Riveline et al. (1996), which distinguished an early Barremian
1031 biozone and a late Barremian biozone. The biozonation by Riveline et al. (1996)
1032 changed the type of biozone from assemblage zones to partial range zones. The
1033 charophyte assemblages observed in successive European biozonations and also in the

European biostratigraphic framework described herein are more diverse but include the assemblages described by Grambast (1974).

Mojon (1996, 2002) questioned the age of these assemblages, suggesting that they were younger (late Barremian and early Aptian, respectively, M8a and M8b) and, therefore, created a third biozone for the early Barremian (M7b) based on a newly defined morphotype, *Globator trochiliscoides* subsp. *mutabilis* (Fig. 6). However, this proposal was based on a misinterpretation of the Barremian units of the Iberian Chain, as discussed by Martín-Closas and Salas (1998). Therefore, the age of these biozones given by Riveline et al. (1996) is now supported by the calibration of the charophyte assemblages performed with SIS in the present study. As a consequence, the two European biozones proposed herein, i.e., the Globator maillardii var. trochiliscoides and the Ascidiella cruciata-Pseudoglobator paucibracteatus biozones, can be largely correlated with the equivalent biozones of Riveline et al. (1996) (Fig. 6).

Barremian charophyte biozonations have been proposed for two more regions, China and South America (Argentina). In China, two Barremian assemblage biozones were proposed by Wang and Lu (1982): the Perimneste ancora-Clypeator jiuquanensis and the Atopochara trivolvis triquetra-Flabellochara hebeiensis biozones. The age of these biozones was used as a reference for subsequent biostratigraphic proposals (e.g., Peng et al. 2003, Yang et al. 2008). With the exception of *C. grovesii* var. *jiuquanensis* (= *Clypeator jiuquanensis*), which is now considered to date to the late Barremian-early Aptian (also in China according to Li et al. 2020), the association described within the Perimneste ancora-Clypeator jiuquanensis biozone has been documented in Europe through the Globator maillardii var. steinhauseri European biozone (see Riveline et al. 1996), which dates to the latest Berriasian–late Hauterivian. By contrast, the clavatoracean assemblage described in the late Barremian Chinese Atopochara trivolvis triquetra-Flabellochara hebeiensis biozone (= *A. trivolvis* var. *triquetra* and *Clavator*

harrisii var. *harrisii*, respectively) by Wang and Lu (1982) is comparable to the European Globator maillardii var. trochiliscoides biozone. The Chinese Atopochara trivolvis triquetra-Flabellochara heibeiensis biozone is also characterised by the presence of *H. neimongolensis* var. *neimongolensis*, suggesting that this Chinese biozone includes the Eurasian Atopochara trivolvis var. triquetra and Hemiclavator neimonglensis var. neimongolensis biozones proposed herein.

In Argentina, a late Hauterivian–early Barremian Atopochara trivolvis triquetra assemblage zone was proposed by Musacchio (1989, 2000). This biozone is characterised by the association of *A. trivolvis triquetra* (= *A*. *trivolvis* var. *triquetra*) with *Triclypella patagonica* Musacchio (synonym of *Clavator calcitrapus* var. *jiangluoensis*, see Pérez-Cano et al. 2020). The association of *A*. *trivolvis* var. *triquetra* with *C*. *calcitrapus* var. *jiangluoensis* is observed in the European G. maillardii var. trochiliscoides biozone (section 7.1) and in the Eurasian A. trivolvis var. triquetra and H. neimongolensis var. neimongolensis biozones (section 7.2), making the correlation between South Amerian and Eurasian basins possible. A late Barremian biozone has not yet been characterised in South America. The Aptian South American Flabellochara harrisii (= C. harrisii var. harrisii) biozone distinguished by Musacchio (1989, 2000) can be partially correlated with the European Ascidiella cruciata-Pseudoglobator paucibracteatus biozone and with the Eurasian Clavator grovesii var. jiuquanensis biozone.

8.3. Correlations with the marine realm

The $^{87}Sr/^{86}Sr$ ratios and derived numerical ages can be used to correlate charophyte assemblages with ammonite biozonations. This correlation was carried out by taking into account the $^{87}Sr/^{86}Sr$ values reported by different studies for the Tethyan and Boreal domains, as well as the standard $^{87}Sr/^{86}Sr$ curve found in the 'LOWESS 5 fit

1086 26 03 13' look-up table of McArthur, which is tied to the numerical ages and ammonoid
1087 biozonation of the GTS2012 by Gradstein et al. (2012). However, the offset between the
1088 Boreal and Tethyan Barremian $^{87}Sr/^{86}Sr$ curves (see Mutterlose et al., 2014) makes the
1089 precise correlation between the Tethyan and Boreal domains difficult for this stage.
1090 The stratigraphically lowest sample analysed for SIS (OyFr21c) coincides with
1091 the FAD of *H. neimongolensis* var. *neimongolensis* in the Fredes section (Fig. 4) and,
1092 thus, with the base of the homonymous Eurasian biozone. The $^{87}Sr/^{86}Sr$ ratio of this
1093 sample, 0.707481 (see Table 2), is similar to the $^{87}Sr/^{86}Sr$ ratios (0.707478 to 0.707483)
1094 reported from southern France by Bodin et al. (2009) between the upper part of the
1095 *Nicklesia pulchella* and the lower part of the *Kotetishvilia compressissima* ammonoid
1096 biozones. According to the Sr isotope curve tied to the GTS2012 used, this $^{87}Sr/^{86}Sr$
1097 ratio correlates precisely with the boundary between the *N. pulchella* and *K.*
1098 *compressissima* ammonoid biozones (Fig. 6). McArthur et al. (2004) reported $^{87}Sr/^{86}Sr$
1099 ratios of ~0.707476 to ~0.707485 for the early Barremian *Haplocrioceras fissicostatum*
1100 Zone of the Boreal region.
1101 The stratigraphically upper samples for SIS were obtained from the Artoles
1102 Formation in the Herbers-Mas de Petxí section. Sample OyH4 was obtained 5 metres
1103 above the FAD of *P. paucibracteatus* with a Sr isotope value of 0.707482, and was used
1104 to date the base of the Ascidiella cruciata-Pseudoglobator paucibracteatus biozone. A
1105 similar value of 0.707483 has been described for the lower part of the *K.*
1106 *compressissima* Tethyan ammonite biozone in south-eastern France (Bodin et al. 2009).
1107 In addition, plotting the Sr isotope value obtained from sample OyH4 against the
1108 standard Sr isotope curve from the GTS2012 revealed a correlation with the *K.*
1109 *compressissima* Zone. Hence, the Sr isotope data confirm the hypothesis of Martín-
1110 Closas et al. (2009), who indirectly correlated the base of the Cruciata-Paucibracteatus
1111 biozone with the middle part of the *Holcodiscus caillaudianus* ammonite biozone (late

1112 early Barremian). This ammonite biozone was relegated to a subzone inside the *K.*
1113 *compressissima* Zone in the most recent proposal of ammonite zonation for the West
1114 Mediterranean Province of the Tethyan Realm (Reboulet et al. 2018). The Sr isotope
1115 value obtained with sample OyH4 coincides with those of the *Haplocrioceras*
1116 *fissocostatum* ammonite biozone in the Boreal Realm (values from 0.707476 to
1117 0.707485; see McArthur et al. 2004).

1118 OyH6 was the youngest low-Mg sample used to derive the numerical ages in this
1119 study (Fig. 3B). The sample has an $^{87}Sr/^{86}Sr$ value of 0.707489 (Table 2), which
1120 corresponds to a period from late early Barremian to early late Barremian (*sensu* Wan et
1121 al. 2019). This period is associated with stable $^{87}Sr/^{86}Sr$ ratios (e.g., Jones and Jenkins,
1122 2001, McArthur et al. 2012, Mutterlose et al. 2014), making it difficult to obtain a
1123 precise numerical age within this interval. The Sr isotope value of sample OyH6 falls
1124 within the range (0.707485-0.707493) obtained by McArthur et al. (2004) for the
1125 *Paracrioceras elegans* ammonite biozone in the Boreal Realm. Bodin et al. (2009) and
1126 Huck et al. (2011) reported similar mean $^{87}Sr/^{86}Sr$ values for the Tethyan Realm as
1127 those found here for the *Moutoniceras moutonianum* ammonite biozone (latest early
1128 Barremian) and the base of the *Toxancyloceras vandenheckii* (earliest late Barremian)
1129 ammonite biozone. According to the Sr isotope curve tied to the GTS2012, the $^{87}Sr/^{86}Sr$
1130 value of sample OyH6 correlates with that of the early late Barremian Tethyan
1131 *Toxancyloceras vandenheckii* ammonite biozone (Fig. 6). However, sample OyH6 was
1132 obtained ~24.5 m below the FAD of *C. grovesii* var. *jiuquanensis* (Fig. 3B).
1133 Consequently, the base of the homonymous biozone may be younger than the numerical
1134 age obtained for this sample.

1135

1136 **9. Conclusions**

Compiled biogeographic and biostratigraphic data on clavatoracean species, with a particular focus on its succession recorded in the Maestrat Basin, established two distinct charophyte biozonations (European and Eurasian) spanning the Barremian-early Aptian period. The European charophyte biozonation is composed of two biozones whose index species were endemic in the Cretaceous Tethyan Archipelago. Its application is currently restricted to present-day Europe and North Africa. The biozones correspond to the Globator maillardii var. trochiliscoides (early Barremian) and Ascidiella cruciata-Pseudoglobator paucibracteatus (late early Barremian–early Aptian) biozones. The novel Eurasian biozonation proposed here includes the Atopochara trivolvis var. triquetra (early Barremian), Hemiclavator neimongolensis var. neimongolensis (late early Barremian–early late Barremian) and Clavator grovesii var. jiuquanensis (late Barremian–early Aptian) biozones. This new biostratigraphic proposal, whose index species are widely reported throughout Eurasia, aims to facilitate the correlation between distant continental basins (e.g., from China and Europe).

Correlation between the continental and marine realms carried out using $^{87}Sr/^{86}Sr$ values indicated that the age of the boundary between the Globator maillardii var. trochilicoides and Ascidiella cruciata-Pseudoglobator paucibracteauts biozones of the European biozonation is roughly equivalent to that of the lower part of the Tethyan *Kotetishvilia compressissima* ammonoid biozone (*c*. 129.70 Ma). Regarding the Eurasian biozonation, the age of the base of the Hemiclavator neimongolensis var. neimongolensis biozone, which bounds the Atopochara trivolvis var. triquetra biozone below, correlates with that of the boundary between the *Nicklesia pulchella* and *Kotetishvilia compressissima* ammonite zones (*c*. 129.80 Ma). The base of the Clavator grovesii var. jiuquanensis biozone is constrained to the upper part of the *Toxancyloceras vandenheckii* ammonoid Zone (*c*. 129.00–128.63 Ma).

The five Barremian biozones described in this paper (including the European and Eurasian biostratigraphic frameworks) have been recognised in the stratigraphic succession studied in Herbers-Mas de Petxí. Therefore, we propose this sedimentary record cropping out in the northern Maestrat Basin to be the main reference section for Barremian charophyte biostratigraphy.

Acknowledgements

This study was supported by project BIOGEOEVENTS (CGL2015-69805-P) via the Spanish Ministry of Economy and Competitiveness, the European Regional Development Fund (ERDF) and project 2017SGR-824 of AGAUR (Catalan Research Agency). The research was also supported by the predoctoral grant BES-2016-076469 from the Spanish Ministry of Economy and Competitiveness to JP-C.

Dr Alejandro Gallardo and Jordi Illa are acknowledged for their laboratory assistance during the sample processing. We would like to thank Francisco Menéndez, Rubén Martínez, and Maria Teresa González (CCiTUB) for their laboratory assistance during the OES-MS analysis. We are also grateful to José Manuel Fuenlabrada (CAI de Ciencias de la Tierra y Arqueometría, Universidad Complutense de Madrid) for his assistance with the isotope analysis. The authors are grateful to the editor Dr. Jochen Erbacher, the reviewer Dr. Alba Vicente (Estación Regional del Noroeste–Universidad Nacional Autónoma de México) and to an anonymous reviewer for their comments and the suggestions that significantly improved the manuscript. The English language of the manuscript was corrected by Michael Maudsley, University of Barcelona (Fundació Bosch i Gimpera, Universitat de Barcelona).

References

1187 Alonso-Zarza, A.M., Calvo, J.P., 2000. Palustrine sedimentation in an
1188 episodically subsiding basin: the Miocene of the northern Teruel Graben (Spain).
1189 Palaeogeography, Palaeoclimatology, Palaeoecology **160 (1–2)**, 1–21.
1190 Alonso-Zarza, A.M.,Wright, V.P., 2010. Palustrine carbonates. In Alonso-Zarza
1191 A.M., Tanner, L.H. (Eds), Carbonates in continental settings: facies, environments and
1192 processes. Developments in Sedimentology, vol. 61. Elsevier, Amsterdam, p. 103–131.
1193 Bádenas, B., Aurell, M., Gasca, J.M., 2018. Facies model of a mixed-clastic,
1194 wave-dominated open-coast tidal flat (Tithonian–Berriasian, north-east Spain).
1195 Sedimentology **65 (5)**, 1631–1666.
1196 Benito, M.I., Suárez-González, P., Quijada, E.I., Campos-Soto, S., Rodríguez-
1197 Martínez, M., 2020. Constraints of applying strontium isotope stratigraphy in coastal
1198 and shallow marine environments: insights from Lower Cretaceous Carbonates
1199 deposited in an active tectonic setting (N Iberian Basin, Spain). Journal of Iberian
1200 Geology. https://doi.org/10.1007/s41513-020-00142-z
1201 Bodin, S., Fiet, N., Godet, A., Matera, V., Westermann, S., Clément, A., Janssen,
1202 N.M.M., Stille, P., Föllmi, K.B., 2009. Early Cretaceous (late Berriasian to early
1203 Aptian) palaeoceanographic change along the northwestern Tethyan margin (Vocontian
1204 Trough, southeastern France): $\delta^{13}C$, $\delta^{18}O$ and Sr-isotope belemnite and whole-rick
1205 records. Cretaceous Research **30**, 1247–1262.
1206 Boix, C., Frijia, G., Vicedo, V., Bernaus, J.M., Di Lucia, M., Parente, M., Caus,
1207 E., 2011. Larger foraminifera distribution and strontium isotope stratigraphy of the La
1208 Cova limestones (Coniacian–Santonian, “Serra del Montsec”, Pyrenees, NE Spain).
1209 Cretaceous Research **32**, 806–822.
1210 Bover-Arnal, T., Strasser, A. 2013. Relative sea-level change, climate and
1211 sequence boundaries: insights from the Kimmeridgian to Berriasian platform carbonates
1212 of Mount Salève (E France). International Journal of Earth Sciences **102 (2)**, 493–515.

1213 Bover-Arnal, T., Moreno-Bedmar, J.A., Frijia, G., Pascual-Cebrian, E., Salas, R.,
1214 2016. Chronostratigraphy of the Barremian-Early Albian of the Maestrat Bain (E
1215 Iberian): integrating strontium-isotope stratigraphy and ammonoid biostratigraphy.
1216 Newsletters on Stratigraphy **49 (1)**, 41–68.
1217 Brand, U., Veizer, J., 1980. Chemical diagenesis of a multicomponent carbonate
1218 system: 1. Trace elements. Journal of Sedimentary Petrology **50**, 1210–1236.
1219 Brasier, M.D., Rozanov, A. Yu., Zhuravlev, A. Yu., Corfield, R.M., Derry, L.A.,
1220 1994. A carbon isotope reference scale for the Lower Cambrian succession in Siberia:
1221 report of IGCP Project 303. Geological Magazine **131 (6)**, 767–783.
1222 Canérot, J., Leyva, F., 1978. Mapa y memoria explicativa de la Hoja Peñarroya de
1223 Tastavins (nº 520) del Mapa Geológico de España a escala 1:50.000. Instituto
1224 Geológico y Minero de España, Madrid, 42 p.
1225 Canérot, J., Cugny, P., Pardo, G., Salas, R., Villena, J., 1982. Ibérica Central-
1226 Maestrazgo. In García, A. (Ed.), El Cretácico de España. Universidad Complutense de
1227 Madrid, Madrid, p. 273–344.
1228 Caus, E., Frijia, G., Parente, M., Robles-Salcedo, R., Villalonga, R., 2016.
1229 Constraining the age of the last marine sediments in the late Cretaceous of central south
1230 Pyrenees (NE Spain): Insights from larger benthic foraminifera and strontium isotope
1231 stratigraphy. Cretaceous Research **57**, 402–413.
1232 Climent-Domènech, H., Martín-Closas, C., Salas, R., 2009. Charophyte-rich
1233 microfacies in the Barremian of the Eastern Iberian Chain (Spain). Facies **55**, 387–400.
1234 Combes, P.J., 1969. Recherches sur la genèse des bauxites dans le Nord-Est de
1235 l'Espagne, le Languedoc and l'Ariège (France). PhD Thesis University of Montpellier.
1236 Montpellier (France), 378 p.
1237 Combes, P.J., Glaçon, G., Grambast, L. 1966. Observations stratigraphiques et
1238 paléontologiques sur le Crétacé inférieur du NE du Maestrazgo (Espagne). Comptes

1239 Rendus Sommaire des Séances de la Société Géologique de France Séance **10**, 390–
1240 391.
1241 Denison, R.E., Koepnick, R.B., Fletcher, A., Howell, M.W., Callaway, W.S.
1242 1994. Criteria for the retention of original seawater in ancient shelf limestones.
1243 Chemical Geology (Isotope Geoscience Section) **112**, 131–143.
1244 Feist, M., Lake, R.D., Wood, C.J., 1995. Charophyte biostratigraphy of the
1245 Purbeck and Wealden of Southern England. Palaeontology **38**, 407–442.
1246 Freytet, P., Plaziat, J.C., 1982. Continental Carbonate Sedimentation and
1247 Pedogenesis–Late Cretaceous and Early Tertiary of Southern France. E.
1248 Schweizerbart'sche Verlagsbuchhandlung (Nägele u. Obermiller). Stuttgart. 213 p.
1249 Frijia, G., Parente, M., Di Lucia, M., Mutti., 2015. Carbon and strontium isotope
1250 stratigraphy of the Upper Cretaceous (Cenomanian–Campanian) shallow-water
1251 carbonates of southern Italy: Chronostratigraphic calibration of larger foraminifera
1252 biostratigraphy. Cretaceous Research **53**, 110–139.
1253 Galbrun, B., Feist, M., Colombo, F., Rocchia, R., Tambareau, Y., 1993.
1254 Magnetostratigraphy and biostratigraphy of Cretaceous-Tertiary continental deposits,
1255 Ager Basin, Province of Lérida, Spain. Palaeogeography, Palaeoclimatology,
1256 Palaeoecology **102**, 41–52.
1257 Gale, A.S., Mutterlose, J., Batenburg, S., 2020. The Cretaceous Period. In
1258 Gradstein, F.M., Ogg, J.G., Schmitz, M.D., Ogg, G.M (Eds). Geologic Time Scale
1259 2020. Elsevier Science Limited, Amsterdam, p. 1023–1086.
1260 Gàmez, D., Paciotti, P., Colombo, F., Salas, R., 2003. La Formación Arcillas de
1261 Morella (Aptiense inferior), Cadena Ibérica oriental (España) caracterización
1262 sedimentológica. Geogaceta **34**, 191–194.
1263 García, R, Moreno-Bedmar, J.A., Bover-Arnal, T., Company, M., Salas, R., Latil,
1264 J.L., Martín-Martín, J.D., Gómez-Rivas, E., Bulot, L.G., Delanoy, G., Martínez, R.,

García de Domingo, A., López-Olmedo, F., 1985. Mapa y memoria explicativa de la hoja de Beceite (nº 521) del Mapa Geológico de España a escala 1:50.000. Instituto Geológico y Minero de España, Madrid, 41 p.

Gierlowski-Kordesch, E.H., 2010. Lacustrine Carbonates. In Alonso-Zarza A.M., Tanner, L.H. (Eds), Carbonates in continental settings: facies, environments and processes. Developments in Sedimentology, vol. 61. Elsevier, Amsterdam, p. 1–101.

Gong, Z., van Hinsbergen, D.J.J., Dekkers, M.J., 2009. Diachronous pervasive remagnetization in northern Iberia during the Cretaceous rotation and extension. Earth and Planetary Science Letters **284**, 292–301.

González-León, O., Ossó, À., Bover-Arnal, T., Moreno-Bedmar, J.A., Frijia, G., Vega, F.J., 2017. *Atherfieldastacus rapax* (Harbort, 1905) (Glypheidae, Mecochiridae) from the Lower Cretaceous of the Maestrat Basin (NE Spain). Cretaceous Research **77**, 56–68.

Gradstein, F.M. Ogg, J.G., Schmitz, M.D., Ogg, G.M., 2012. The geologic Time Scale 2012. Elsevier, Amsterdam, 1144.

Gradstein, F.M. Ogg, J.G., Schmitz, M.D., Ogg, G.M., 2020. Geologic Time Scale 2020. Elsevier, Amsterdam, 1347.

Grambast, L., 1966a. Un nouveau type structural chez les Clavatoracées, son intérêt phylogénetique et stratigraphique. Comptes Rendus des Séances de l'Académie des Sciences, Paris D **262**, 1929–1932.

Grambast, L., 1966b. Structure de l'utricule et phylogénie chez les Clavatoracées. Comptes Rendus des Séances de l'Académie des Sciences, Paris D **262**, 2207–2210.

Grambast, L., 1967. La série évolutive *Perimneste-Atopochara* (Charophytes). Comptes Rendus des Séances de l'Académie des Scienes, Paris **264**, 581–584.

1289 Grambast, L., 1968. Evolution of the utricle in the charophyta genera *Perimneste*
1290 Harris and *Atopochara* Peck. Journal of the Linnean Society (Botany) **61**, 5–11.
1291 Grambast, L., 1969. La symétrie de l'utricule chez les Clavatoracées et sa
1292 signification phylogénétique. Comptes Rendus Académie des Sciences, Paris **269**, 878–
1293 881.
1294 Grambast, L., 1970. Origine et évolution des *Clypeator* (Charophytes). Comptes
1295 Rendus des Séances de l'Académie des Sciences, Paris **271**, 1964–1967.
1296 Grambast, L., 1974. Phylogeny of the Charophyta. Taxon **23**, 463–481.
1297 Guimerà, J., 2018. Structure of an intraplate fold-and-thrust belt: The Iberian
1298 Chain. A synthesis. Geologica Acta **16**, 427–438.
1299 Horikx, M., Heimhofer, U., Dinis, J., Huck, S., 2014. Integrated stratigraphy of
1300 shallow marine Albian strata from the southern Lusitanian Basin of Portugal.
1301 Newsletters on Stratigraphy **47(1)**, 85–106.
1302 Huck, S., Heimhofer, U., Rameil, N., Bodin, S., Immenhauser, A., 2011.
1303 Strontium and carbon-isotope chronostratigraphy of Barremian-Aptian shoal-water
1304 carbonates: Northern Tethyan platform drowning predates OAE 1a. Earth and Planetary
1305 Science Letters **304**, 547–558.
1306 Jones, C.E., Jenkins, H.C., 2001. Seawater strontium isotopes, oceanic events and
1307 seafloor hydrothermal activity in the Jurassic and Cretaceous. American Journal of
1308 Science **301**, 112–149.

1309 Li, S. Wang, Q., Zhang, H., Lu, H., Martín-Closas, C., 2016. Charophytes from
1310 the Cretaceous – Paleogene transition in the Pingyi Basin (Eastern China) and their
1311 Eurasian correlation. Cretaceous Research **59**, 179–200.

1312 Li, S., Wang, Q., Zhang, H., Wan, X., Martín-Closas, C., 2019. Charophytes from
1313 the Cretaceous–Paleocene boundary in the Songliao Basin (North-Eastern China): a

1314 Chinese biozonation and its calibration to the geomagnetic polarity time scale. Papers in
1315 Palaeontology **5 (1)**, 47–81.
1316 Li, S., Wang, Q., Zhang, H., 2020. Charophytes from the Lower Cretaceous
1317 Xiagou Formation in the Jiuquan Basin (northwestern China) and their
1318 palaeogeographical significance. Cretaceous Research **105**, 103940.
1319 Martín-Chivelet, J., López-Gómez, J., Aguado, R., Arias, C., Arribas, J., Arribas,
1320 M.E., Aurell, M., Bádenas, B., Benito, M.I., Bover-Arnal, T., Casas-Sainz, A., Castro,
1321 J.M., Coruña, F., de Gea, G.A., Fornós, J.J., Fregenal-Martínez, M., García-Senz, J.,
1322 Garófano, D., Gelabert, B., Giménez, J., González-Acebrón, J., Guimerà, J., Liesa, C.L.,
1323 Mas, R., Meléndez, N., Molina, J.M., Muñoz, J.A., Navarrete, R., Nebot, M., Nieto,
1324 L.M., Omodeo-Salé, S., Pedrera, A., Peropadre, C., Quijada, I.E., Quijano, M.L.,
1325 Reolid, M., Robador, A., Rodríguez-López, J.P., Rodríguez-Perea, A., Rosales, I., Ruiz-
1326 Ortiz, P.A., Sàbat, F., Salas, R., Soria, A.R., Suárez-González, P., Vilas, L., 2019. The
1327 Late Jurassic–Early Cretaceous Rifting. In: Quesada, C., Oliveira, J.T. (Eds.), The
1328 Geology of Iberia: A Geodynamic Approach. Volume 3: The Alpine Cycle. Springer,
1329 Heidelberg, pp. 60–63.
1330 Martín-Closas, C. 1989. Els caròfits del Cretaci inferior de les conques
1331 perifèriques del Bloc de l'Ebre, PhD Thesis, Universitat de Barcelona, Barcelona, Spain
1332 608 p.
1333 Martín-Closas, C., 1996. A phylogenetic system of Clavatoraceae (Charophyta).
1334 Review of Palaeobotany and Palynology **94**, 259–293.
1335 Martín-Closas, C., 2000. Els caròfits del Juràssic superior i Cretaci inferior de la
1336 Península Ibèrica. Arxius de les Seccions de Ciències. Institut d'Estudis Catalans, 125,
1337 Barcelona, 304 p.

1338 Martín-Closas, C., 2015. Cosmopolitanism in Northern Hemisphere Cretaceous
1339 Charophyta (Clavatoroidae). Palaeogeography, Palaeoclimatology, Palaeoecology **438**,
1340 9–23.

1341 Martín-Closas, C., Grambast-Fessard, N., 1986. Les charophytes du Crétacé
1342 inférieur de la région du Maestrat (Chaîne Ibérique, Catalanides, Espagne).
1343 Paléobiologie Continentale **15**, 1–66.

1344 Martín-Closas, C., Salas, R., 1988. Corrélation de la bizonation des Charophytes
1345 avec celle des Foraminifères (Orbitolinidés) dans le Valanginien inférieur du Bassin du
1346 Maestrat (Castelló, Espagne). Geobios **21 (5)**, 645–650.

1347 Martín-Closas, C., Salas, R., 1994. Lower Cretaceous Charophytes.
1348 Biostratigraphy and evolution in the Maestrat Basin (Eastern Iberian Ranges). VIII
1349 Meeting of the European Group of Charophyte Specialists Fieldtrip Guidebook,
1350 Diagonal, Barcelona, 89 p.

1351 Martín-Closas, C., Salas, R., 1998. Lower Cretaceous charophyte biozonation in
1352 the Maestrat Basin (Iberian Ranges, Spain). A reply to P.O. Mojon. Géologie Alpine **74**,
1353 97–110.

1354 Martín-Closas, C., Alonso-Millán, A., 1998. Estratigrafía y bioestratigrafía
1355 (Charophyta) del Cretácico inferior en el sector occidental de la Cuenca de Cameros
1356 (Cordillera Ibérica). Revista de la Sociedad Geológica de España **11**, 253–269.

1357 Martín-Closas, C., Wang. Q., 2008. Historical biogeography of the lineage
1358 *Atopochara trivolvi*s Peck 1941 (Cretaceous Charophyta). Palaeogeography
1359 Palaeoclimatology Palaeoecology **260**, 435-451.

1360 Martín-Closas, C., Wang. Q., 2010. Historical biogeography of Clavatoraceae. In:
1361 Gailis, M., Kalnins, S (Eds.). Biogeography. Nova Science. New York, 203–217.

1362 Martín-Closas, C., Clavel, B., Charollais, J., Conrad, M.A., 2009. Charophytes
1363 from the Barremian-lower Aptian of the Norhtern Subalpine Chains and Jura
1364 Mountains, France: correlation with associated marine assemblages. Cretaceous
1365 Research **30**, 49–62.
1366 McArthur, J.M. Howarth, R.J. Bailey, T.R., 2001. Strontium isotope stratigraphy:
1367 lowess version 3. Best-fit to the marine Sr-isotope curve for 0 to 509 Ma and
1368 accompanying look-up table for deriving numerical age. Journal of Geology **109**, 155–
1369 170.

1370 McArthur, J.M., Muttelose, J., Price, G.D., Rawson, P.F., Ruffell, A., Thirlwall,
1371 M.F., 2004. Belemnites of Valanginian, Hauterivian and Barremian age: Sr-isotope
1372 stratigraphy, composition ($^{87}Sr/^{86}Sr$, $\delta^{13}C$, $\delta^{18}O$, Na, Sr, Mg) and palaeo-oceanography.
1373 Palaeogeography, Palaeoclimatology, Palaeoecology **202**, 253–272.

1374 McArthur, J.M. Howarth, R.J., Shields, G.A., 2012. Strontium isotope
1375 stratigraphy. In Gradstein, F.M., Ogg, J.G., Schmitz, M., Ogg, G. (Eds.), The
1376 Geological Time Scale. Elsevier Science Limited, p. 127–144.

1377 McArthur, J.M., Howarth, R.J., Shields, G.A., Zhou, Y. 2020. Strontium Isotope
1378 Stratigraphy. In Gradstein, F.M., Ogg, J.G., Schmitz, M.D., Ogg, G.M (Eds). Geologic
1379 Time Scale 2020. Elsevier Science Limited, Amsterdam, p. 211–238.

1380 Meléndez, M.N., Liesa, C.L., Soria, A.R., Meléndez, A., 2009. Lacustrine system
1381 evolution during early rifting: El Castellar Formation (Galve sub-basin, Central Iberian
1382 Chain). Sedimentary Geology **222**, 64–77.
1383 Mojon, P.O., 1988. Les dépôts émersifs des faciès urgoniens (Hauterivien
1384 supérieur-Aptien inférieur) dans le Jura Méridional (Ain, France) et les Chaînes

1385 subalpines septentrionales (Haute-Savoie, Savoie et Isère, France). Archives des
1386 Sciences, Genève **41**, 409–417.
1387 Mojon, P.O., 1996. Précisions sur l'intervalle Valanginien-Barrémien de la
1388 biozonation des Charophytes du Crétacé inférieur du Maestrazgo (Chaîne Ibérique
1389 Orientale, Espagne) et sur la biozonation des Charophytes de l'intervalle Jurassique
1390 supérieur-Crétacé de l'Europe occidentale. Géologie Alpine **72**, 61–99.
1391 Mojon, P.O. 2002. Les formations mésozoiques à Charophytes (Jurassique
1392 moyen-Crétacé inferieur) de la marge téthysienne nor-occidentale (Sud-est de la France,
1393 Suisse occidentale, nord-est de l'Espagne). Sédimentologie, micropaléontologie,
1394 biostratigraphie. Géoplogie Alpine. Mémoire Hors Série 41, 386 p.
1395 Moreau, M.G., Canérot, J., Malod, J.A., 1992. Paleomagnetic study of Mesozoic
1396 sediments from the Iberian Chain (Spain). Suggestions for Barremian remagnetization
1397 and implications for the rotation of Iberia. Bulletin de la Société Géologique de France
1398 **163 (4)**, 393–402.
1399 Musacchio, E.A., 1989. Biostratigraphy of non-marine Cretaceous of Argentina
1400 based on Calcareous microfossils. In: Wiedmann, J. (Ed.), Cretaceous of the Western
1401 Tethys, Proceedings of the 3rd International Cretaceous Symposium, Tübingen 1987. E.
1402 Schweizerbart'sche Verlagsbuchhandlung, Stuttgart, pp. 811–850.
1403 Musacchio, E.A., 2000. Biostratigraphy and biogeography of Cretaceous
1404 Charophytes from South America. Cretaceous Research **21**, 211–220.
1405 Mutterlose, J., Bodin, S., Fähnrich, L., 2014. Strontium-isotope stratigraphy of the
1406 Early Cretaceous (Valanginian–Barremian): Implications for Boreal–Tethys correlation
1407 and paleoclimate. Cretaceous Research **50**, 252–263.
1408 Nebot, M., Guimerà, J., 2016. Structure of an inverted basin from subsurface and
1409 field data: the Late Jurassic-Early Cretaceous Maestrat Basin (Iberian Chain). Geologica
1410 Acta **14 (2)**, 155–177.

1411 Ogg, J.G., Hinnov, L.A., 2012. Cretaceous. In Gradstein, F.M., Ogg, J.G.,
1412 Schmitz, M., Ogg, G. (Eds.), The Geological Time Scale. Elsevier Science Limited,
1413 Amsterdam, p. 793–853.

1414 Peng, W.S., Wang, Q.F., Xue, D., Lu, H.N., Zhang, F., 2003. Cretaceous
1415 charophytes from the Inggen-Ejinaqi Basin of the Inner Mongolia. Acta
1416 Micropalaeontologica Sinica **20**, 365–376. (in Chinese).

1417 Pérez-Cano, J., Bover-Arnal, T., Martín-Closas, C., 2020. Barremian charophytes
1418 from the Maestrat Basin. Cretaceous Research **115**, 104544.
1419 Platt, N.H., 1989. Lacustrine carbonates and pedogenesis: sedimentology and
1420 origin of palustrine deposits from the Early Cretaceous Rupelo Formation. W Cameros
1421 Basin, N Spain. Sedimentology **36**, 665–684.
1422 Reboulet, S., Szives, O., Aguirre-Urreta, B., Barragán, R., Company, M., Frau, C.,
1423 Kakabadze, M.V., Klein, J., Moreno-Bedmar, J.A., Lukeneder, A., Pictet, A., Ploch, I.,
1424 Raisossadat, S., Vašíček, Z., Baraboshkin, E.J., Mitta, V.V., 2018. Report on the 6th
1425 International Meeting of the IUGS Lower Cretaceous Ammonite Working Group
1426 (Vienna, Austria, 20th August 2017. Cretaceous Research **91**, 100–110.
1427 Riveline, J., Berger, J.P., Bilan, W., Feist, M., Martín-Closas, C., Schudack, M.,
1428 Soulié-Märsche, I., 1996. European Mesozoic-Cenozoic charophyte biozonation.
1429 Bulletin de la Société Géologique de France **167 (3)**, 453–468.
1430 Rosales, I., Quesada, S., Robles, S., 2001. Primary and diagenetic isotopic signals
1431 in fossils and hemipelagic carbonates: the Lower Jurassic of northern Spain.
1432 Sedimentology **48 (5)**, 1149–1169.
1433 Salas, R., 1987. El Malm i el Cretaci inferior entre el Massís de Garraf i la Serra
1434 d'Espadà. Anàlisi de Conca. PhD Thesis. Universitat de Barcelona, Barcelona. 345 p.

Salas, R., Casas, A., 1993. Mesozoic extensional tectonics, stratigraphy and crustal evolution during the Alpine Cycle of the Eastern Iberian Basin. Tectonophysics **228**, 33–55.

Salas, R., Guimerà, J., 1996. Rasgos estructurales principales de la cuenca cretácica inferior del Maestrazgo (Cordillera Ibérica oriental). Geogaceta **20 (7)**, 1704–1706.

Salas, R., Guimerà, J., Mas, R., Martín-Closas, C., Meléndez, A., Alonso, A., 2001. Evolution of the Mesozoic Central Iberian Rift System and its Cainozoic inversion (Iberian Chain). In: Ziegler, P.A., Cavazza, W., Roberston, A.H.F., Crasquin-Soleau, S., (eds.), Peri-Tethys Memoir 6: Peri-Tethyan Rift/Wrench Basins and Passive Margins. Mémoires du Muséum National d'Histoire Naturelle, Paris, p. 145–186.

Sanjuan, J., Martín-Closas, C., Costa, E., Barberà, X., Garcès, M., 2014. Calibration of Eocene-Oligocene charophyte biozones in the Eastern Ebro Basin (Catalonia, Spain). Stratigraphy **11 (1)**, 61–81.

Sanjuan, J., Vicente, A., Pérez-Cano, J., Stoica, M., Martín-Closas, C. 2021. Early Cretaceous charophytes from south Dobrogea (Romania). Biostratigraphy and palaeobiogeography. Cretaceous Research, **122**: 104702.

Schneider, S., Fürsich, F.T., Werner, W., 2009. Sr-isotope stratigraphy of the Upper Jurassic of central Portugal (Lusitanian Basin) based on oyster shells. International Journal of Earth Science (Geologische Rundschau) **98**, 1949–1970.

Schudack, M.E., 1987. Charophytenflora und fazielle Entwicklung der Grenzschichten mariner Jura/Wealden in den Nordwestlichen Iberischen Ketten (mit Vergleichen zu Asturien und Kantabrien). Palaeontographica Abteilung B **204**, 1–108.

Schudack, M.E., 1993. Die Charophyten im Oberjura und Unterkreide Westeuropas. Mit einer phylogenetischen Analyse der Gesamtgruppe. Berliner Geowissenschaftliche Abhandlungen (A) **8**, 209 p.

1461 Steuber, T., 1999. Isotopic and chemical intra-shell variations in low-Mg calcite
1462 of rudists bivalves (Mollusca: Hippuritacea): disequilibrium fractionations and Late
1463 Cretaceous seasonality. International Journal of Earth Sciences **88**, 551–570.
1464 Steuber, T., 2001. Strontium isotope stratigraphy of Turonian-Campanian Gosau-
1465 type rudists formation in the Norhtern Calcareous and Central Alps (Austria and
1466 Germany). Cretaceous Research **22**, 429–441.
1467 Steuber, T., Korbar, T., Jelaska, V., Gušić, I., 2005. Strontium isotope stratigraphy
1468 of Upper Cretaceous platform carbonates of the island of Brac (Adriatic Sea, Croatia):
1469 implications for global correlation of platform evolution and biostratigraphy.
1470 Cretaceous Research **26**, 741–756.
1471 Suárez, M.B., Ludvigson, G.A., González, L.A., Al-Suwaidi, A.H., You, H.L.,
1472 2013. Stable isotope chemostratigraphy in lacustrine strata of the Xiagou Formation,
1473 Gansu Province, NW China. Geological Society, London, Special Publication **382**, p.
1474 143–155.

1475 Trabelsi, K., Soussi, M., Touir, J., Houla, J., Abbes, C., Martin-Closas, C., 2016.
1476 Charophytenbiostratigraphy of the non-marine Lower Cretaceous in the Central
1477 Tunisian Atlas (North Africa): Palaeobiogeographic implications. Cretaceous Research
1478 **67**, 66–83.
1479 Tucker, M.E., 1985. Shallow-marine carbonate facies and facies models.
1480 Geological Society, London, Special Publications **18 (1)**, 147-169.
1481 Vicente, A., Martín-Closas, C., 2013. Lower Cretaceous charophytes from the
1482 Serranía de Cuenca, Iberian chain: Taxonomy, biostratigraphy and palaeoecology.
1483 Cretaceous Research **40**, 227–242.
1484 Vicente, A., Martín-Closas, C., Arz, J.A., Oms, O., 2015. Maastrichtian-basal
1485 Paleocene charophyte biozonation and its calibration to the Global Polarity Time Scale
1486 in the southern Pyrenees (Catalonia, Spain). Cretaceous Research **52**, 268–285.

1487 Vicente, A., Villalba-Breva, S., Ferrández-Cañadell, C., Martín-Closas, C., 2016.
1488 Revision of the Maastrichtian-Palaeocene charophyte biostratigraphy of the Fontllonga
1489 reference section (southern Pyrenees, Catalonia, Spain). Geologica Acta **14(4)**, 349–
1490 362.
1491 Wan, R., Wenjan, L., McArthur, J.M., Wang, Z., 2019. Sr-isotope chronology of
1492 carbonate rocks: Quantifying the uncertainty of inversion. In Montenari, E. (Eds.),
1493 Stratigraphy and Timescales 4: Case studies in isotope stratigraphy. Elsevier Limited
1494 Science, p. 35–72.
1495 Wang, Z., Lu, H.N., 1982. Classification and evolution of Clavatoraceae with
1496 notes on its distribution in China. Bulletin Nanjing Institute of Geology and
1497 Paleontology. Academia Sinica **4**, 77–104 (in Chinese).
1498 Wenzel, B., 2000. Differential preservation of primary isotopic signatures in
1499 Silurian brachiopods. Journal of Sedimentary Research **70 (1)**, 194–209.
1500 Williamson, T., Henderson, R.A., Price, G.D. Collerson, K.D., 2012. Strontium-
1501 isotope stratigraphy of the Lower Cretaceous of Australia. Cretaceous Research **36**, 24–
1502 36.
1503 Yang, J.L., Wang, Q.F., Lu, H.N., 2008. Cretaceous charophyte floras from the
1504 Junggar Basin, Xinjiang, China. Acta Micropalaeontologica Sinica **25 (4)**, 345–363. (in
1505 Chinese).
1506

Figure captions

Figure 1. A) Map of the main structural units of the Iberian Peninsula (modified from Salas et al. 2001). B) Palaeogeographical map of the Late Jurassic-Early Cretaceous syn-rift Maestrat and Garraf basins (modified from Salas et al. in Martín-Chivelet et al. 2019). SB, Sitges Sub-basin; EMB, El Montmell Sub-basin; EPB, El Perelló Sub-basin; SaB, Salzedella Sub-basin; OrB, Orpesa Sub-basin; PGB, Penyagolosa Sub-basin; CB, Cedramán Sub-basin; GB, Galve Sub-basin; LPB, Las Parras Sub-basin; OlB, Oliete Sub-basin; MoB, Morella Sub-basin. C) Geological map of the Herbers-Mas de Petxí area showing the location of the section logged (modified from Canérot and Leyva 1978). D) Geological map of the area of Fredes showing the location of the section logged (modified from García de Domingo and López-Olmedo 1985).

Figure 2. Lithostratigraphy of the uppermost Jurassic–Lower Cretaceous record of the Morella Sub-basin (after Salas et al. 2001, Bover-Arnal et al. 2016).

Figure 3A. Stratigraphic log of the lower part of the Herbers-Mas de Petxí section showing the location from where the samples were obtained and the distribution of the charophyte species. Charophyte biostratigraphy follows the new biozonations presented here. Geographical and geological location shown in Fig. 1C. See Figure 5 for legend.

Figure 3B. Stratigraphic log of the upper part of the Herbers-Mas de Petxí section showing the location from where samples were obtained and the distribution of the charophyte species. Charophyte biostratigraphy follows the new biozonations presented here. Geographical and geological location shown in Figure 1C. See Figure 5 for the legend.

Figure 4. Stratigraphic log of the Fredes section. Charophyte biostratigraphy follows the new biozonations presented here. Geographical and geological location are shown in Figure 1D. See Figure 5 for the legend.

1533 Figure 5. Key for Figures 3A–B and 4.

1534 Figure 6. European and Eurasian Barremian charophyte biozones and their
1535 calibrated numerical ages. Numerical ages and geomagnetic polarity were obtained
1536 from Gradstein et al. (2012). Ammonite biostratigraphy was taken from Reboulet et al.
1537 (2018) and the age ranges for the ammonite biozones were obtained from Ogg and
1538 Hinnov (2012). The previous Barremian–early Aptian European biozones (Grambast
1539 1974, Feist et al. 1995, Mojon 1996, 2002, Riveline et al, 1996, Martín-Closas et al.
1540 2009) and Chinese biozones (Wang and Lu 1982, Yang et al. 2008) are compared with
1541 those proposed in the present study, considering only the charophyte biozones and the
1542 age given by the different studies and not the absolute ages. The correlation with
1543 ammonite biozones was only well-established by Riveline et al. (1996) and Martín-
1544 Closas et al. (2009). The dashed line in the Eurasian C. grovesii var. jiuquanensis
1545 biozone (present study) represents the maximum numerical age of this biozone.

1546

1547 Table 1: Charophyte species identified in the Herbers-Mas de Petxí and Fredes
1548 sections (the Morella Sub-basin). Letters A-H and A-E are referring to the intervals
1549 described in sections 5.1 and 5.2. L: Laterite.

1550 Table 2. Analytical results and the derived numerical ages obtained from the low-
1551 Mg calcite oyster shells analysed in the present study. See Figures 3A–B and 4 for the
1552 location from where the analysed samples were obtained. The numerical ages follow
1553 those of Gradstein et al. (2012) and are derived from the 'LOWESS 5 fit 26 03 13'
1554 look-up table by McArthur, and those of Gradstein et al. (2020) derived from the
1555 'LOESS 6 16 03 2020' by McArthur (personal communication, 2021). ± 2 s.e., standard
1556 error; N.A., not analysed; Deg.Alt., degree of alteration; D.Alt., diagenetically-altered;
1557 Fr.Alt., freshwater-altered; N.Alt., non-altered. Samples and the analytical results used
1558 to derive the numerical ages are shown in bold.

1559

1560 Plate 1. A) *Porochara maestratica* (lateral view; sample H8; specimen no. 85579
1561 MGSCB); B) *P. maestratica* (apical view; sample H8; specimen no. 85580 MGSCB);
1562 C) aff. *Mesochara harrisii* (lateral view; sample H39; specimen no. 85585 MGSCB);
1563 D) aff. *M. harrisii* (apical view; sample H39; specimen no. 85586); E) *Echinochara*
1564 *lazarii* (external cast of the gyrogonite; sample H95; specimen no. 85589 MGSCB); F)
1565 *E. lazarii* (inner series of the utricle; sample H94; specimen no 85592 MGSCB); G) *E*
1566 *lazarii* (outer series of the utricle; sample H88; specimen no. 85601 MGSCB); H)
1567 *Globator maillardii* var. *trochiliscoides* (lateral view; sample H27; specimen no. 85602
1568 MGSCB); I) *G. maillardii* var. *biutricularis* (lateral view; sample H44; specimen no.
1569 85605 MGSCB); J) *Atopochara trivolvis* var. *triquetra* (lateral view; sample H51;
1570 specimen no. 85608); K) *A. trivolvis* var. *trivolvis* (lateral view; sample H94; specimen
1571 no. 85611 MGSCB); L) *Clavator grovesii* var. *gautieri* (lateral view; sample FR27;
1572 specimen no. 85651 MGSCB); M) *C. grovesii* var. *gautieri* (adaxial view; sample
1573 FR27; specimen no. 85678 MGSCB); N) *C. grovesii* var. *jiuquanensis* (lateral view;
1574 sample H95; specimen no. 85614 MGSCB); O) *C. grovesii* var. *jiuquanensis* (adaxial
1575 view; sample H88; specimen no. 85616 MGSCB); P) *C. harrisii* var. *dongjingensis*
1576 (lateral view; sample H38; specimen no. 85617 MGSCB); Q) *C. harrisii* var. *harrisii*
1577 (lateral view; sample H38; specimen no. 85620 MGSCB); R) *C. harrisii* var. *reyi*
1578 (lateral view; sample H76; specimen no. 85622 MGSCB); S) *C. calcitrapus* var.
1579 *jiangluoensis* (apical view; sample H38; specimen no. 85623 MGSCB); T) *C.*
1580 *calcitrapus* var. *calcitrapus* (apical view; sample H51; specimen no. 85626 MGSCB).

1581 Plate 2. A) *Ascidiella stellata* var. *stellata* (lateral view; sample H6; specimen no.
1582 85677 MGSCB); B) *A. stellata* var. *stellata* (apical view; sample H6; specimen no.
1583 85630 MGSCB); C) *A. stellata* var. *lata* (lateral view; sample H44; specimen no. 85632
1584 MGSCB); D) *A. stellata* var. *lata* (apical view; sample H44; specimen no. 86633

MGSCB); E) *Ascidiella triquetra* (lateral view; sample H27; specimen no. 85636 MGSCB); F) *A. triquetra* (apical view; sample H27; specimen no. 85637 MGSCB); G) *A. cruciata* (abaxial view; sample H94; specimen no. 85638 MGSCB); H) *A. cruciata* (apical view; sample H94; specimen no. 85639); I) *Hemiclavator adnatus* (adaxial view; sample H12; specimen no. 85641 MGSCB); J) *H. adnatus* (lateral view; sample H12; specimen no. 85642 MGSCB); K) *H. neimongolensis* var. *posticecaptus* (adaxial view; sample H12; specimen no. 85644 MGSCB); L) *H. neimongolensis* var. *posticecaptus* (lateral view; sample H12; specimen no. 85645); M) *H. neimongolensis* var. *neimongolensis* (adaxial view; sample H39; specimen no. 85648 MGSCB); N) *H. neimongolensis* var. *neimongolensis* (lateral view; sample H39; specimen no. 85649 MGSCB); O) *Pseudoglobator paucibracteatus* (lateral view; sample H96; specimen no. 85650 MGSCB).

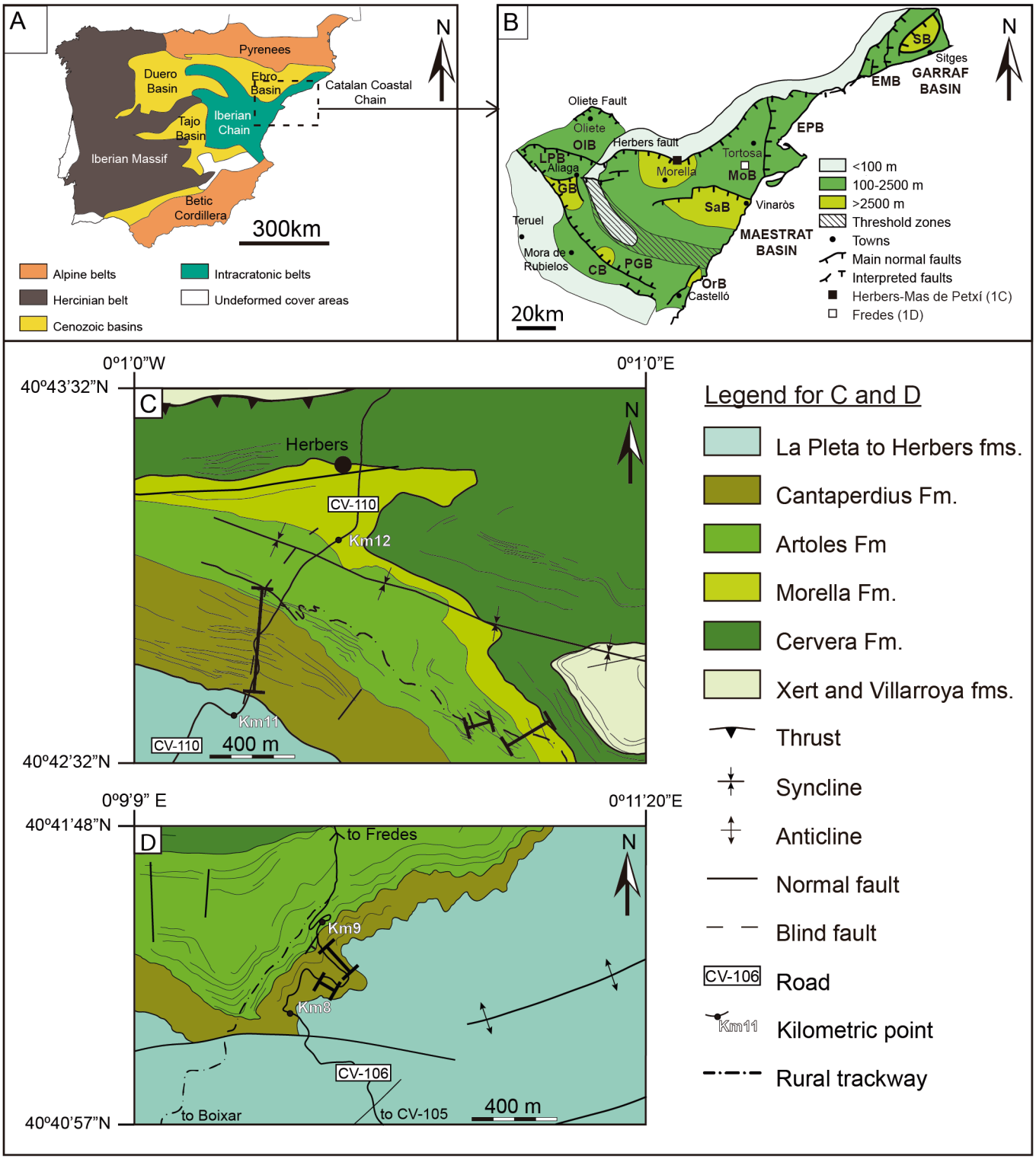
A
Pyrenees
Duero Basin
Ebro Basin
Catalan Coastal Chain
Tajo Basin
Iberian Chain
Iberian Massif
Betic Cordillera
300km
N
Alpine belts
Hercinian belt
Cenozoic basins
Intracratonic belts
Undeformed cover areas
B
SB
Sitges
EMB
GARRAF BASIN
Oliete Fault
Oliete
OIB
Herbers fault
LPB
Aliaga
GB
Morella
Tortosa
MoB
EPB
SaB
Vinaròs
Teruel
MAESTRAT BASIN
Mora de Rubielos
CB
PGB
OrB
Castelló
20km
<100 m
100-2500 m
>2500 m
Threshold zones
Towns
Main normal faults
Interpreted faults
Herbers-Mas de Petxí (1C)
Fredes (1D)
0º1'0"W
0º1'0"E
40º43'32"N
40º42'32"N
C
Herbers
CV-110
Km12
Km11
CV-110
400 m
0º9'9" E
0º11'20"E
40º41'48"N
40º40'57"N
D
to Fredes
Km9
Km8
CV-106
to Boixar
to CV-105
400 m
Legend for C and D
La Pleta to Herbers fms.
Cantaperdius Fm.
Artoles Fm
Morella Fm.
Cervera Fm.
Xert and Villarroya fms.
Thrust
Syncline
Anticline
Normal fault
Blind fault
CV-106
Road
Km11
Kilometric point
Rural trackway

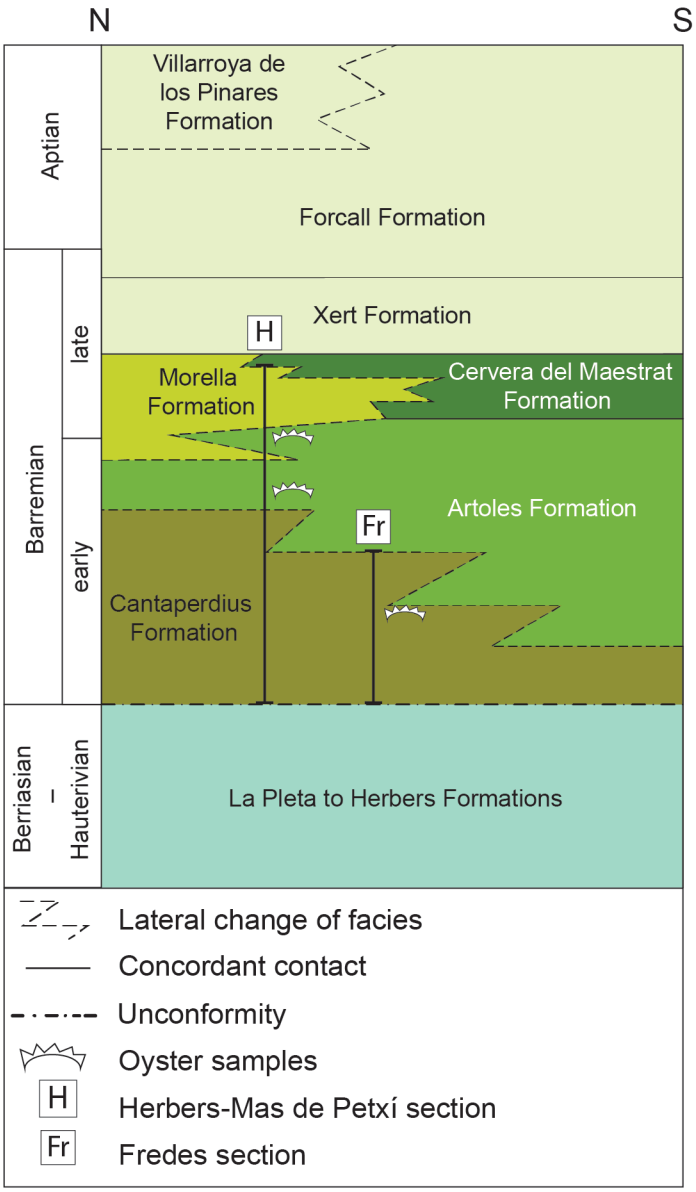
N
S
Aptian
Villarroya de los Pinares Formation
Forcall Formation
Barremian
late
early
Xert Formation
H
Morella Formation
Cervera del Maestrat Formation
Artoles Formation
Fr
Cantaperdius Formation
Berriasian – Hauterivian
La Pleta to Herbers Formations
Lateral change of facies
Concordant contact
Unconformity
Oyster samples
H
Herbers-Mas de Petxí section
Fr
Fredes section

Lithostratigraphy
Descriptive intervals
Samples
Lithology
Texture and sedimentary structures
Fossils
Porochara maestratica
aff. Mesochara harrisii
Echinochara lazarii
Globator mallardii var. steinhauseri
Globator mallardii var. trochiliscoides
Globator mallardii var. biutricularis
Atopochara. trivolvis var. ancora
Atopochara trivolvis var. triquetra
Clavator harrisii var. dongjingensis
Clavator harrisii var. harrisii
Clavator harrisii var. reyi
Clavator calcitrapus var. jiangluoensis
Clavator calcitrapus var. calcitrapus
Ascidiella stellata var. stellata
Ascidiella stellata var. lata
Ascidiella triquetra
Hemiclavator. adnatus
H. neimongolensis var. posticecaptus
H. neimongolensis var. neimongolensis
European biozonation
Eurasian biozonation
Globator maillardii var. trochiliscoides
Atopochara trivolvis var. triquetra
H. neimongolensis var. neimongolensis
Globator maillardii var. steinhauseri
370
350
300
250
200
150
100
50
0m
Artoles Fm.
Formation
Cantaperdius
D
C
B
A
H56–H57
OyH1
H55
H54
H52–H53
H51
H49–H50
H48
H47b
H46–H47
H42–H45
H41
H38–H40
H37
H36b
H36
H35b
H35
H34
H33
H32
H31b
H30–H31
H29b
H25–H29a
H23–H24
H22
H21
H20b–H20c
H20
H19
H16–H18
H11–H15
H10b–H10f
H8–H10
H7b–H7c
H7
H6e
H6d
H6c
H6b
H6
H5e
H5d
H5c
H5b
H3–H5
H2
H1
Fe
ml
md
wk
pk
gr
Herbers Fm.

Lithostratigraphy
Descriptive Intervals
Samples
Lithology
Texture and sedimentary structures
Fossils
Porochara maestratica
aff. Mesochara harrisii
Echinochara lazarii
Globator mallardii var. trochiliscoides
Globator mallardii var. biutricularis
Atopochara trivolvis var. triquetra
Atopochara trivolvis var. trivolvis
Clavator grovesii var. jiuquanensis
Clavator harrisii var. harrisii
Clavator harrisii var. reyi
Clavator calcitrapus var. calcitrapus
Ascidiella stellata var. lata
Ascidiella triquetra
Ascidiella cruciata
H. neimongolensis var. neimongolensis
Pseudoglobator paucibracteatus
European biozonation
Eurasian biozonation
690
650
600
550
500
450
400
370 m
Morella Formation
Artoles Formation
Morella Fm.
Artoles Formation
H
G
F
E
H 100
H99
H98
H97
H96
H93–H95
H91-H92
H90
H88-H89
H87
H82H–86B
H80-H81
H77–H79
H76
H 75
H 74
H 73
H 71
H 70
H 69
H 68
H 66-H67
H134–H135
H132–H133
H65
H131
H130
H129
H128a–H128b
H62–H64
H127
H126
H125
H124b
H124
H123
H122
H61
H60
H59
H58
H57b
OyH7
OyH6
OyH5
OyH4
OyH3
OyH2
F
ml md wk pk gr
Globator maillardii var. trochiliscoides
Ascidiella cruciata - Pseudoglobator paucibracteatus
Hemiclavator neimongolensis var. neimongolensis
Clavator grovesii var. jiuquanensis

Litostratigraphy
Descriptive intervals
Samples
Lithology
Texture, and sedimentary structures
Fossils
Porochara maestratica
aff. Mesochara harrisii
Echinochara lazarii
Globator maillardii var. steinhauseri
Globator maillardii var. trochiliscoides
Globator mallardii var. biutricularis
Atopochara trivolvis var. triquetra
Clavator grovesii var. gauteri
Clavator harrisii var. dongjingensis
Clavator harrisii var. harrisii
Clavator harrisii var. reyi
Clavator calcitrapus var. jiangluoensis
Clavator calcitrapus var. calcitrapus
Ascidiella stellata var. stellata
Ascidiella stellata var. lata
Ascidiella triquetra
H. neimongolensis var. posticecaptus
H. neimongolensis var. neimongolensis
European biozonation
Eurasian biozonation
Globator maillardi var. trochiliscoides
Hemiclavator neimognolensis ss
Atopochara trivolvis var. triquetra
Globator maillardii var. steinhauseri
98
80
60
40
20m
0m
Cantaperdius Formation
E
D
C
B
A
A
Herbers Fm.
Fr33–Fr34
Fr31–Fr32
Fr29–Fr30
OyFr3
Fr27–Fr28
Fr26c
Fr26b
Fr26
Fr25
Fr23–Fr24
F22
OyFr21c
Fr21c
Fr21c
Fr21b
OyFr2
Fr21b
Fr21
Fr20c
Fr20b
Fr20
Fr19b
Fr19
Fr18b
Fr18
F17d
Fr17b
F17c
F17b
Fr17
Fr16c
Fr16b
Fr16
Fr15
Fr14
Fr12c-Fr13
OyFr1
Fr12b
Fr12
Fr11i–Fr11s
Fr9–Fr10
Fr8
Fr7
Fr6
Fr5
Fr4
Fr3b
Fr3
Fr2
Fr1
F
>1cm
>3cm
ml md wk pk gr

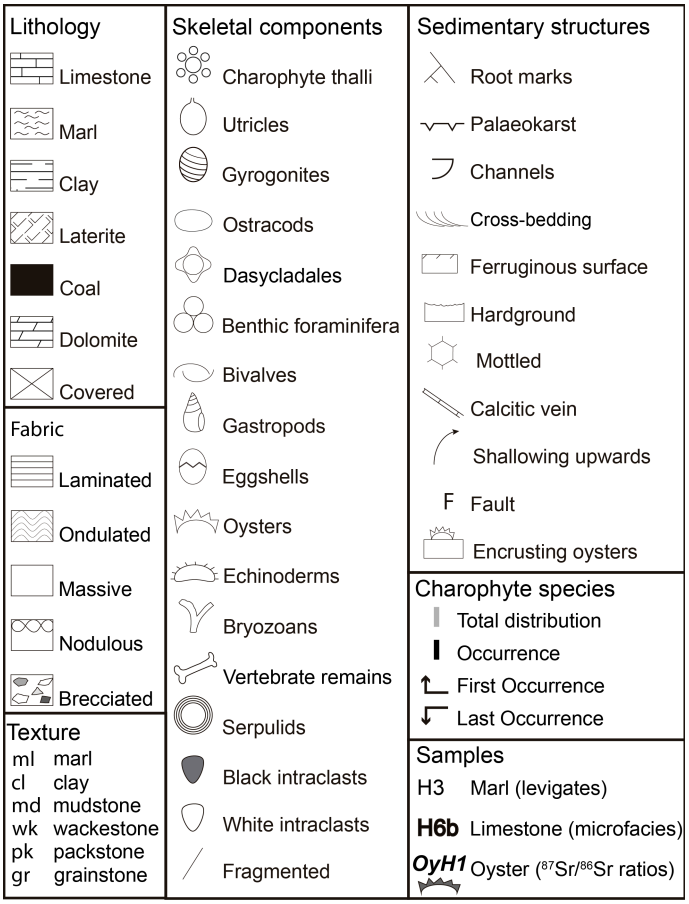
Lithology
Limestone
Marl
Clay
Laterite
Coal
Dolomite
Covered
Fabric
Laminated
Ondulated
Massive
Nodulous
Brecciated
Texture
ml marl
cl clay
md mudstone
wk wackestone
pk packstone
gr grainstone
Skeletal components
Charophyte thalli
Utricles
Gyrogonites
Ostracods
Dasycladales
Benthic foraminifera
Bivalves
Gastropods
Eggshells
Oysters
Echinoderms
Bryozoans
Vertebrate remains
Serpulids
Black intraclasts
White intraclasts
Fragmented
Sedimentary structures
Root marks
Palaeokarst
Channels
Cross-bedding
Ferruginous surface
Hardground
Mottled
Calcitic vein
Shallowing upwards
F Fault
Encrusting oysters
Charophyte species
Total distribution
Occurrence
First Occurrence
Last Occurrence
Samples
H3 Marl (levigates)
H6b Limestone (microfacies)
OyH1 Oyster (87Sr/86Sr ratios)

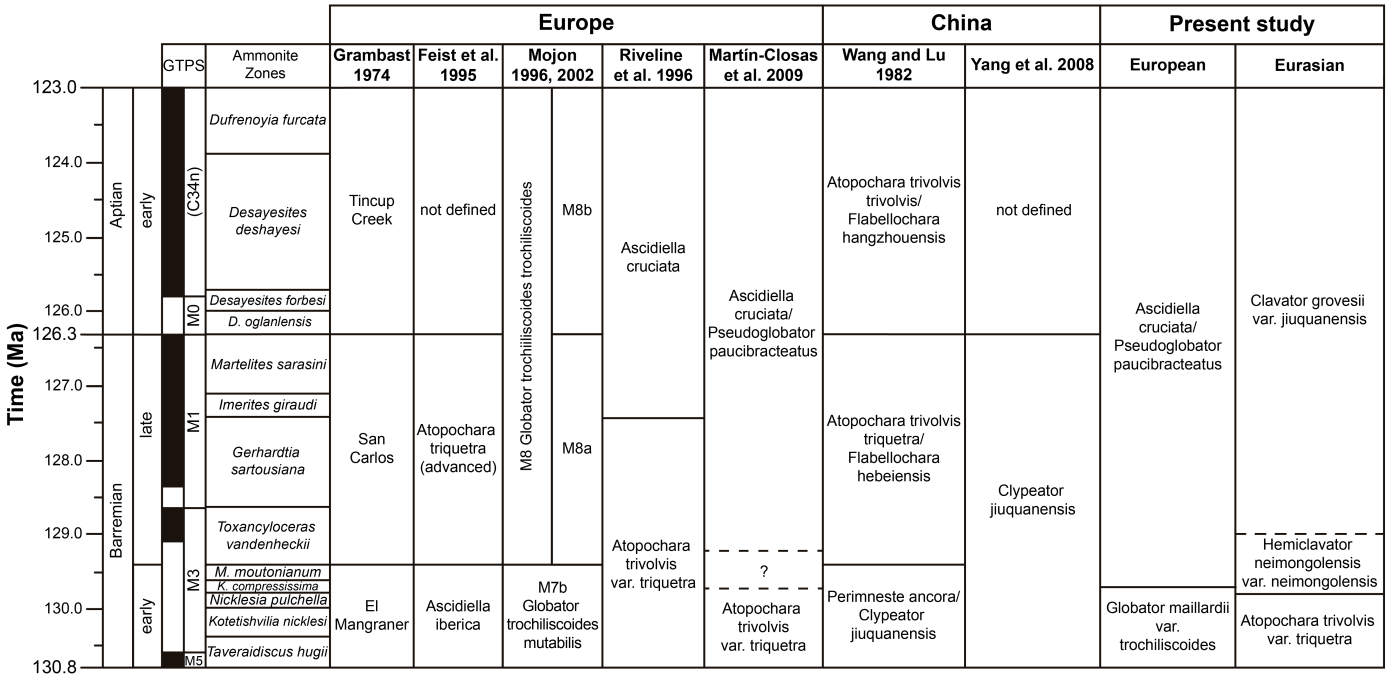
Europe
China
Present study
Time (Ma)
GTPS
Ammonite Zones
Grambast 1974
Feist et al. 1995
Mojon 1996, 2002
Riveline et al. 1996
Martín-Closas et al. 2009
Wang and Lu 1982
Yang et al. 2008
European
Eurasian
123.0
124.0
125.0
126.0
126.3
127.0
128.0
129.0
130.0
130.8
Aptian
Barremian
early
late
early
(C34n)
M0
M1
M3
M5
Dufrenoyia furcata
Desayesites deshayesi
Desayesites forbesi
D. oglanlensis
Martelites sarasini
Imerites giraudi
Gerhardtia sartousiana
Toxancyloceras vandenheckii
M. moutonianum
K. compressissima
Nicklesia pulchella
Kotetishvilia nicklesi
Taveraidiscus hugii
Tincup Creek
not defined
M8 Globator trochiliscoides trochiliscoides
M8b
M8a
Ascidiella cruciata
Ascidiella cruciata/ Pseudoglobator paucibracteatus
Atopochara trivolvis trivolvis/ Flabellochara hangzhouensis
not defined
Ascidiella cruciata/ Pseudoglobator paucibracteatus
Clavator grovesii var. jiuquanensis
San Carlos
Atopochara triquetra (advanced)
Atopochara trivolvis triquetra/ Flabellochara hebeiensis
Clypeator jiuquanensis
Atopochara trivolvis var. triquetra
?
Hemiclavator neimongolensis var. neimongolensis
El Mangraner
Ascidiella iberica
M7b Globator trochiliscoides mutabilis
Atopochara trivolvis var. triquetra
Perimneste ancora/ Clypeator jiuquanensis
Globator maillardii var. trochiliscoides
Atopochara trivolvis var. triquetra

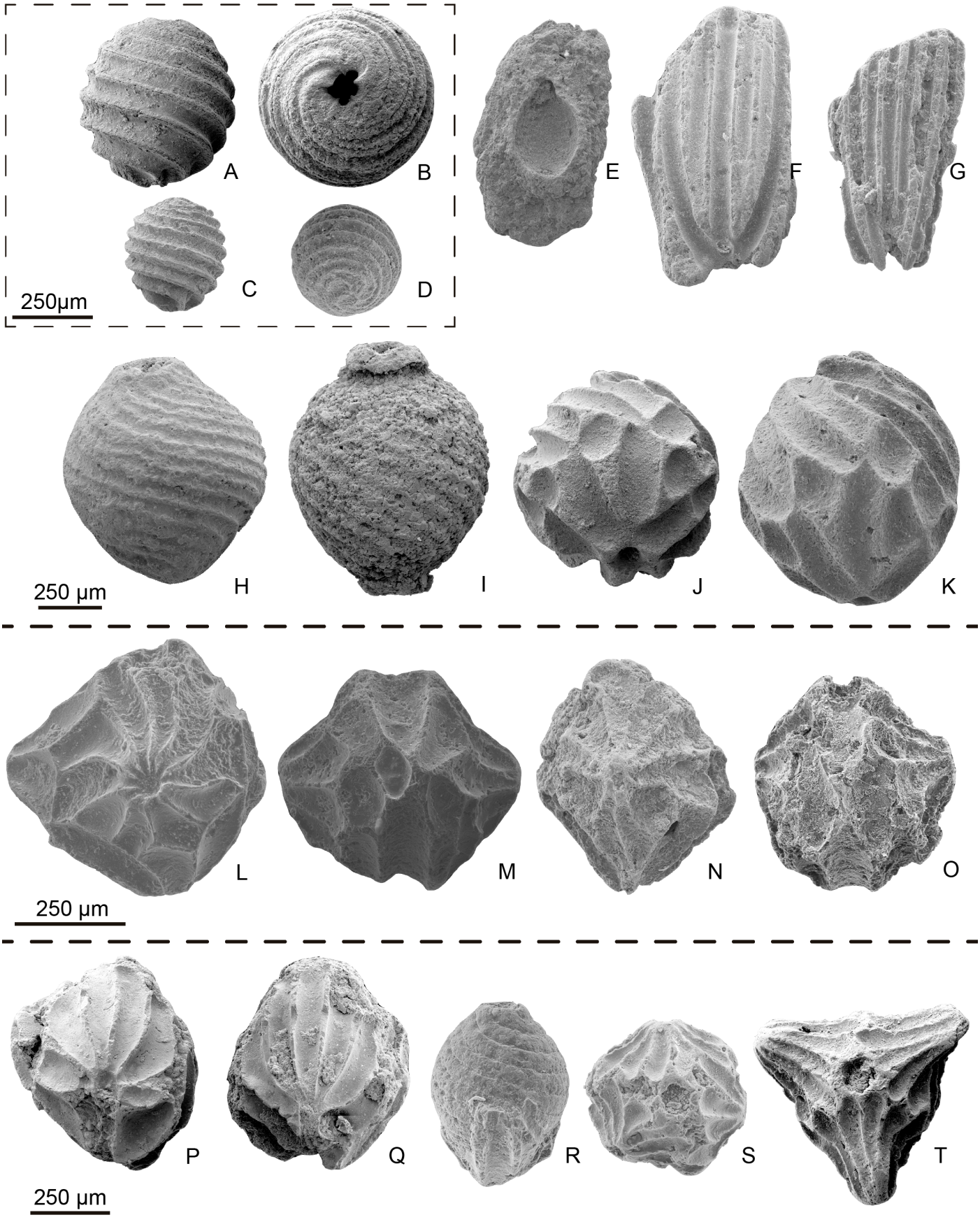
A
B
C
D
250µm
E
F
G
H
I
J
K
250 µm
L
M
N
O
250 µm
P
Q
R
S
T
250 µm

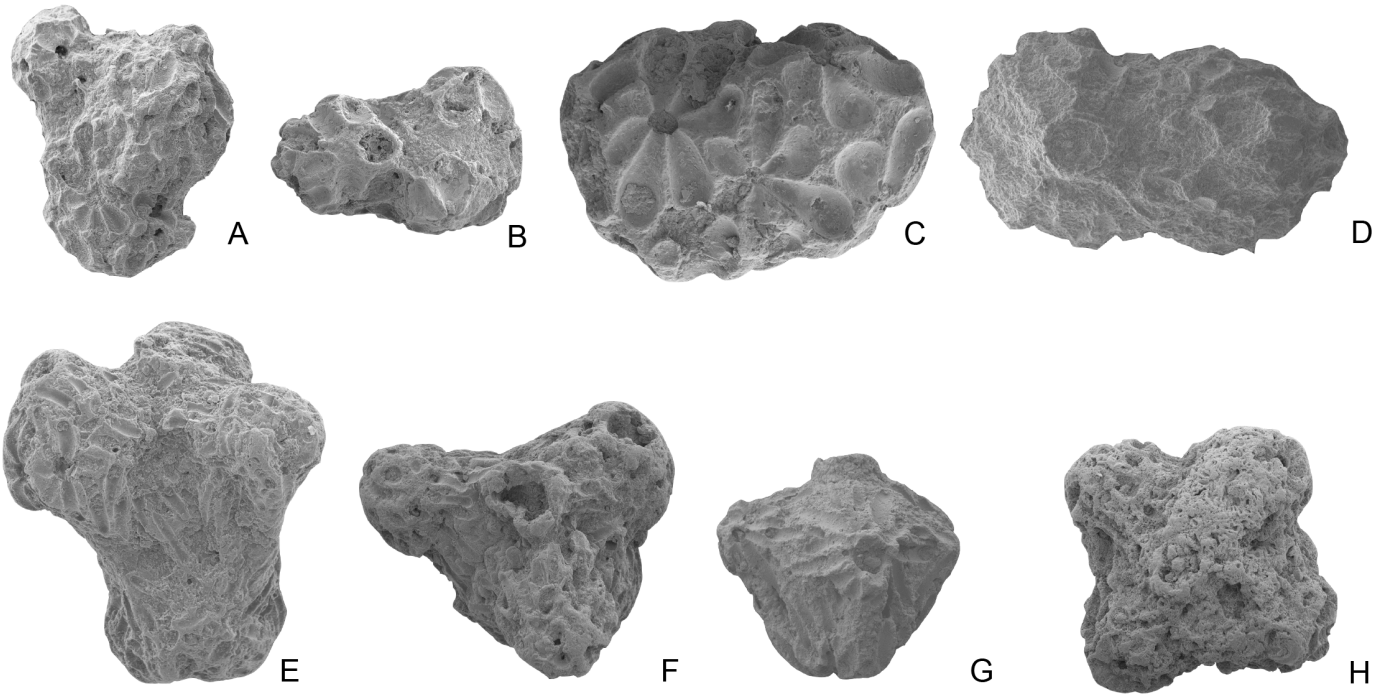
A
B
C
D
E
F
G
H
250 µm

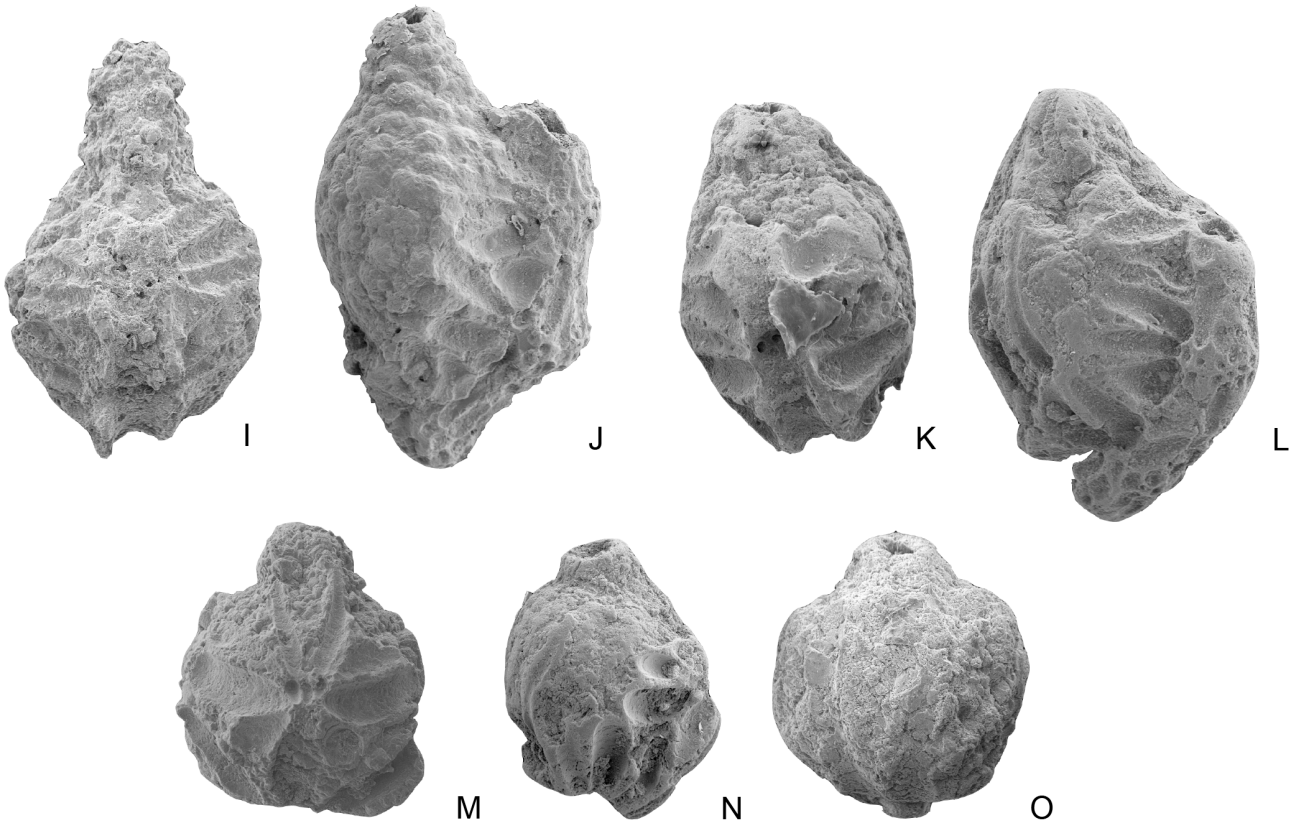
I
J
K
L
M
N
O
250 µm

Table 1

Charophyte fructifications (gyrogonites and utricles)	Herbers-Mas de Petxí									Fredes					
	Intervals									Intervals					
	L	A	B	C	D	E	F	G	H	L	A	B	C	D	E
Family Porocharaceae (Grambast) emend. Schudack															
Genus *Porochara* (Mädler) emend. Schudack															
Porochara maestratica (Martín-Closas et Grambast-Fessard) Schudack		X	X	X	X	X	X				X	X	X	X	X
Family Characeae (Richard ex C. Agardh) emend. Martín-Closas et Schudack															
Genus *Mesochara* Grambast															
aff. *Mesochara harrisii* (Mädler) Shaikin	X	X	X	X	X		X		X	X	X	X	X	X	X
Family Clavatoraceae Pia															
Subfamily Atopocharoidae (Grambast) emend Martín-Closas ex Schudak															
Genus *Echinochara* (Peck) emend. Pérez-Cano, Bover-Arnal et Martín-Closas															
Echinochara lazarii (Martín-Closas) Pérez-Cano, Bover-Arnal et Martín-Closas				X	X	X	X	X	X				X	X	X
Genus *Globator* Grambast															
Globator maillardii var. *trochiliscoides* (Grambast) Martín-Closas		X	X		X		X		X		X	X	X	X	X
Globator maillardii var. *biutricularis* Vicente et Martín-Closas			X		X		X		X			X	X	X	X
Genus *Atopochara* Peck															
Atopochara trivolvis var. *triquetra* (Grambast) Martín-Closas	X	X	X	X	X		X		X	X	X	X	X	X	X
Atopochara trivolvis var. *trivolvis* Peck									X						
Subfamily Clavatoroidae (Grambast) emend. Martín-Closas ex Schudack															
Genus *Clavator* (Reid and Groves) emend. Martín-Closas ex Schudack															
Clavator grovesii var. *gautieri* (Grambast) Martín-Closas														X	X
Clavator grovesii var. *jiuquanensis* (Wang) Grambast, emend. Martín-Closas									X						
Clavator harrisii var. *dongjingensis* (Hu et Zeng) Martín-Closas		X	X		X						X		X		X
Clavator harrisii var. *harrisii* Peck	X	X	X	X	X				X		X	X	X		X
Clavator harrisii var. *reyi* (Grambast-Fessard) Martín-Closas		X	X	X	X		X		X				X	X	X
Clavator calcitrapus var. *jiangluoensis* (Z. Wang et Li in Wang and Lu) Pérez-Cano, Bover-Arnal et Martín-Closas					X										X
Clavator calcitrapus var. *calcitrapus* (Grambast) Martín-Closas ex Schudack					X										X
Genus *Ascidiella* (Grambast) emend. Martín-Closas ex Schudack															
Ascidiella stellata var. *stellata* (Martín-Closas et Grambast-Fessard) Martín-Closas ex Schudack	X	X		X						X	X	X	X		
Ascidiella stellata var. *lata* Martín-Closas		X	X	X	X						X	X	X	X	X
Ascidiella triquetra (Grambast) Martín-Closas	X	X	X	X	X					X	X	X	X	X	X
Ascidiella cruciata (Grambast) Martín-Closas ex Schudack							X	X	X						
Genus *Hemiclavator* Wang et Lu															
Hemiclavator adnatus (Martín-Closas et Grambast-Fessard) Schudack	X	X	X												
Hemiclavator neimongolensis var. *posticecaptus* (Martín-Closas et Grambast-Fessard) Martín-Closas	X	X	X	X	X					X	X	X	X		
Hemiclavator neimongolensis var. *neimonogolensis* Wang et Lu				X	X		X						X	X	X
Genus *Pseudoglobator* Grambast															
Pseudoglobator paucibracteatus Martín-Closas et Grambast-Fessard						X	X		X						

Table 2

	Sample	Lithostratigraphic unit	Mg (ppm)	Sr (ppm)	Mn (ppm)	Fe (ppm)	$^{87}Sr/^{86}Sr$ measured	± 2 s.e.	$^{87}Sr/^{86}Sr$ corrected	Deg. Alt.	Gradstein et al. (2012)			Gradstein et al. (2020)		
											min	Age (MA)	max	min	Age (MA)	max
Herbers-Mas de Petxí	OyH7	Morella Fm.	1133.19	860.74	94.30	467.83	0.707504	0.000012	0.707503	Fr.Alt.						
	OyH6	**Artoles Fm.**	**1300.82**	**855.30**	**101.13**	**248.51**	**0.707490**	**0.000012**	**0.707489**	**N.Alt.**	128.25	**129.00**	129.80	124.20	**125.05**	126.37
	OyH5	Artoles Fm.	3026.78	908.34	291.40	2312.41	0.707543	0.000012	0.707542	Alt.						
	OyH4	**Artoles Fm.**	**1815.09**	**743.62**	**23.31**	**154.04**	**0.707482**	**0.000012**	**0.707482**	**N.Alt.**	129.20	**129.70**	130.90	125.00	**125.35**	126.60
	OyH3	Artoles Fm.	1414.31	959.26	114.33	587.76	0.707515	0.000012	0.707514	Fr.Alt.						
	OyH2	Artoles Fm.	2915.47	711.86	289.95	2503.57	0.707531	0.000012	0.707530	Alt.						
	OyH1	Artoles Fm.	2003.94	831.53	126.41	788.85	0.707513	0.000012	0.707512	Alt.						
Fredes	OyFr3	Artoles Fm.	2237.09	921.57	298.15	546.13	0.707494	0.000012	0.707493	Alt.						
	OyFr21c	**Cantaperdius Fm.**	**281.99**	**2597.47**	**16.36**	**435.94**	**0.707481**	**0.000012**	**0.707481**	**N.Alt.**	129.20	**129.80**	130.95	125.00	**126.10**	126.65
	OyFr2	Cantaperdius Fm.	924.00	810.56	15.53	305.20	0.707442	0.000012	0.707441	Fr.Alt.						
	OyFr1	Cantaperdius Fm.	2440.73	289.22	398.00	4060.16	N.A.			Alt.						